Supplemental Online Content

Xu M, Li X, Teng T, et al. Reconfiguration of structural and functional connectivity coupling in patient subgroups with adolescent depression. *JAMA Netw Open*. 2024;7(3):e241933. doi:10.1001/jamanetworkopen.2024.1933

This supplemental material has been provided by the authors to give readers additional information about their work.

eFigure 1. Study design and analytical procedure

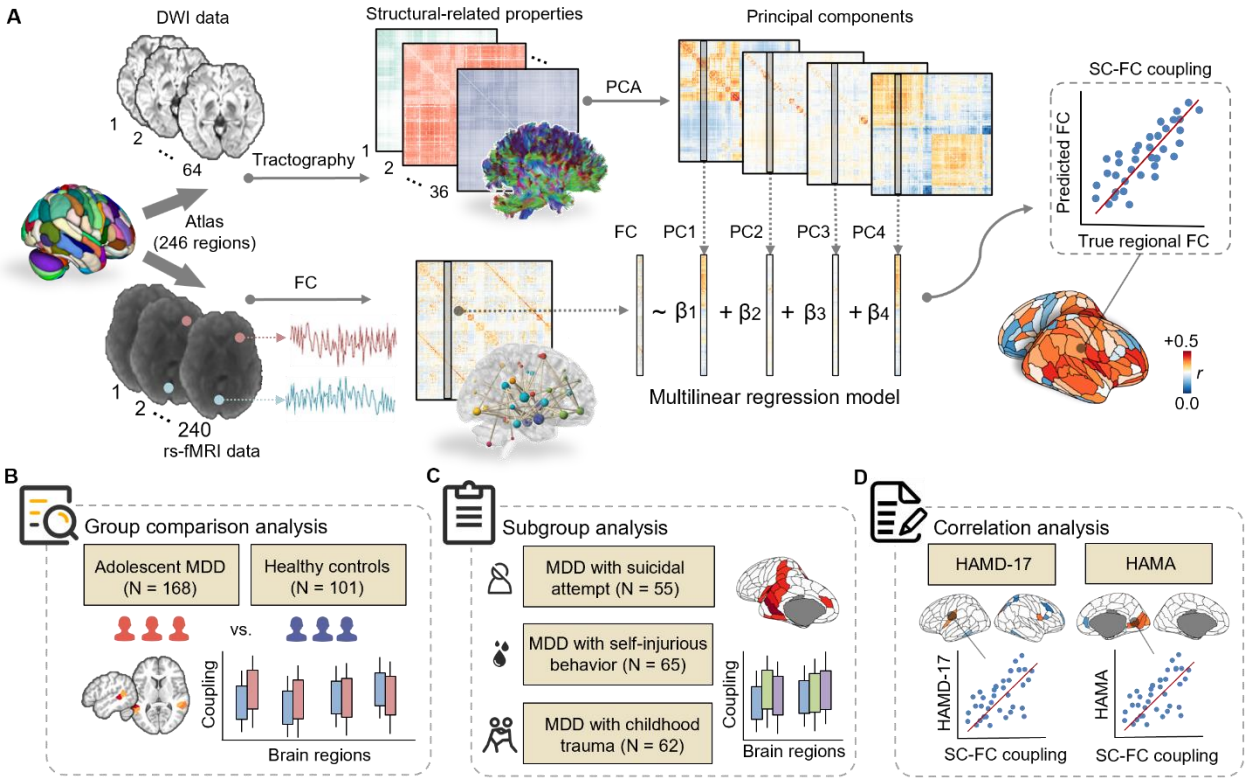

eFigure 1. Study design and analytical procedure. (**A**) The pipeline for calculating the SC-FC coupling of each brain region. First, function connectivity and structure connectivity with 246 brain parcels were calculated for each participant. Second, a suite of structural properties was calculated based on the structure connectivity of each participant. Third, PCA was performed on all 36 structural properties, and the top-n components that collectively accounted for more than 80% of variance were selected. Finally, a multilinear regression model was established based on regional functional profiles and structural profiles of the top-n components, and the SC-FC coupling was measured as the Pearson correlation coefficient of the multilinear model. (**B**) The group difference analysis of the differences of SC-FC coupling in each brain region between adolescent MDD and healthy controls. (**C**) Analysis of the SC-FC coupling variations between MDD subgroups with different clinical characters and healthy controls. (**D**) Correlation analysis between SC-FC coupling and clinical measures, *i.e.*, HAMD-17, HAMA. HAMD-17, 17-item Hamilton Depression Scale; HAMA, Hamilton Anxiety Scale; rs-fMRI, resting-state functional magnetic resonance imaging; DWI, diffusion-weighted imaging; PCA, principal component analysis.

eFigure 2. The pipeline of defining seed and target regions for probabilistic tractography

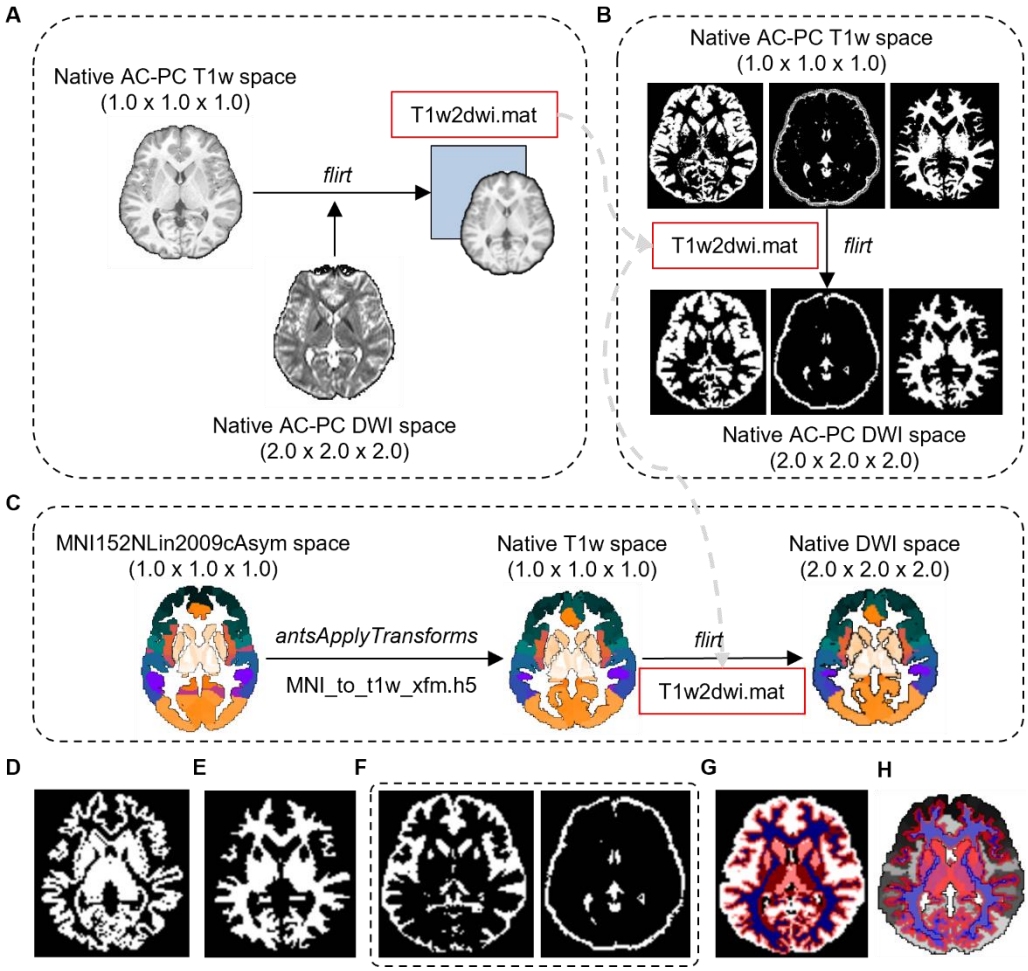

eFigure 2. The pipeline of defining seed and target regions for probabilistic tractography. (**A**) The preprocessed T1w images are registered to the resampled preprocessed DWI reference image ($b = 0$) through FSL's *flirt*, resulting a transformation matrix, *i.e.*, T1w2dwi.mat (from native T1w space to native DWI space). (**B**) GM mask, WM mask, CSF mask are registered to native DWI space through FSL's *flirt* with initialized transformation matrix, *i.e.*, T1w2dwi.mat, thresholding at 0.5. (**C**) The brain atlas is registered to native DWI space through a two−step manner. (**D**) The whole−brain seed mask (in native DWI space) for ROI−by−ROI tractography. (**E**) An example of WM mask in native DWI space. (**F**) Examples of superficial gray mask (the left) and CSF mask (the right). (**G**) Overlay the seed mask on GM mask and WM mask. The red regions correspond to seed mask, the white regions correspond to GM mask, and the blue regions correspond to WM mask. (**H**) Overlay lay the seed mask on the Brainnetome atlas, illustrating the seed voxels of each brain regions.

eFigure 3. Principle component analysis and the consistency of components across participants

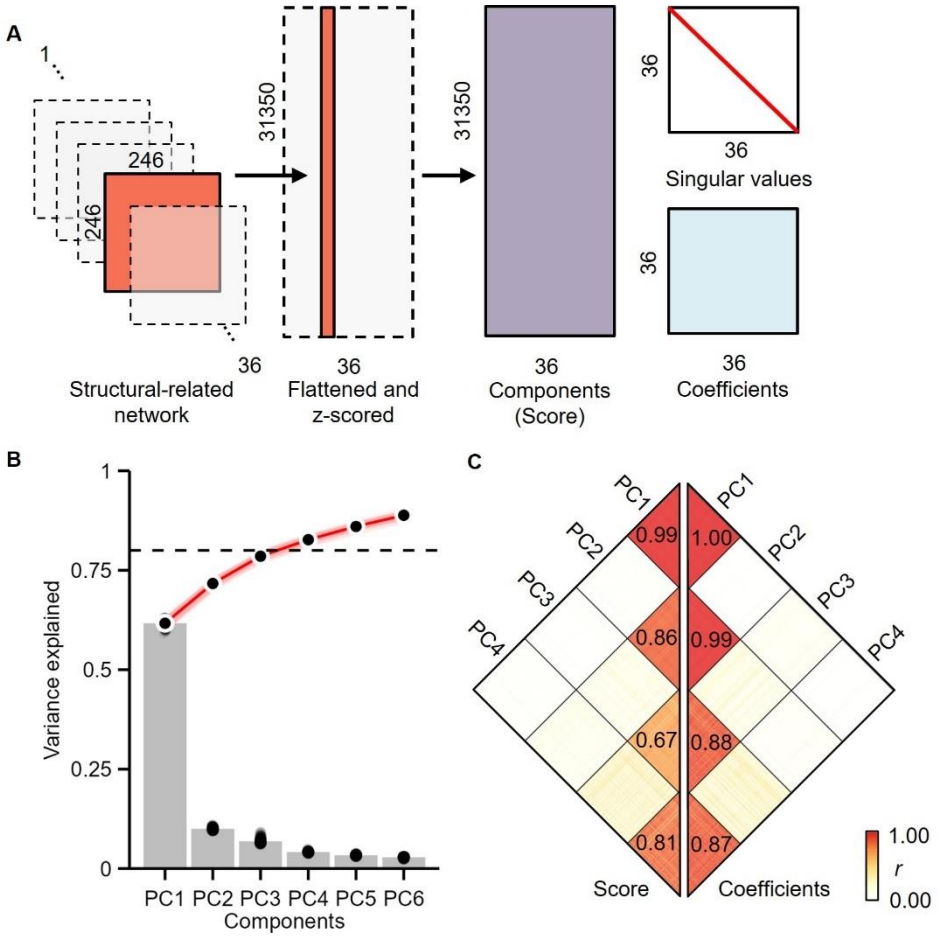

eFigure 3. Principle component analysis and the consistency of components across participants. (**A**) Principal component analysis is performed on flattened 36 structural−related networks. Specifically, each 246×246 symmetrical structural−related matrix is flattened and z−scored, forming a 31350×36 structural feature matrix for each subject. Then, this individual feature matrix is decomposed into (31350×36) principal components (PCs), (36×36) coefficients, (36×36 diagonal) singular values. (**B**) the variance explained of the top 6 principal components. The saturated red line illustrates the mean accumulative variance explained, while light red lines illustrate accumulative explained variance for each participant. The horizontal black dashed line indicates expected 80% variance. Grey bars correspond to the mean variance accounted by each PC, while dark dots correspond to the variance explained by each PC for each participant. Top 4 PCs explain 61.6 ± 0.7, 10.0 ± 0.3, 6.8 ± 0.5, 4.2 ± 0.2 percent of variance, respectively, and collectively explained more than 80% of variance across all participants. (**C**) Similarity analysis of the top 4 PCs. The left part corresponds to the similarity of top 4 PCs, while the right part corresponds to the similarity of coefficients from the top 4 PCs. The similarity is measured as the absolute Pearson correlational coefficient. PC, principal components.

eFigure 4. The pattern and composition of PC1

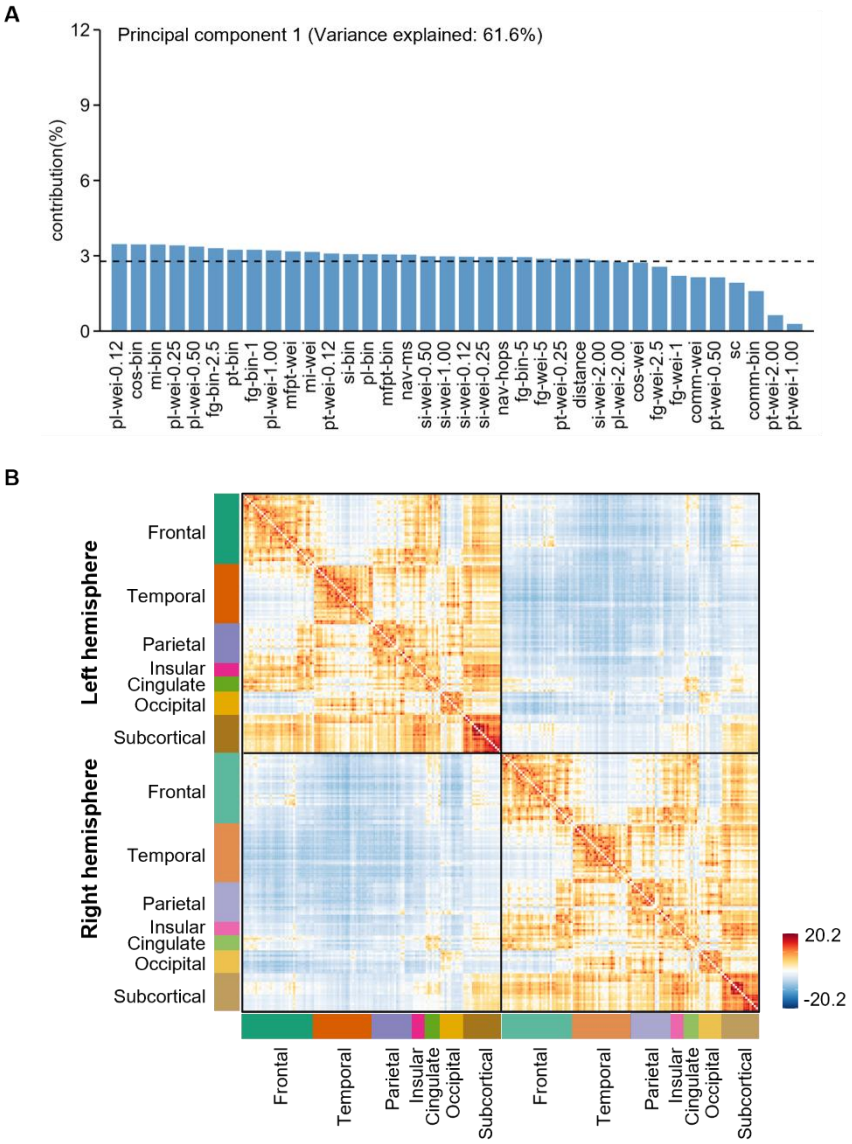

eFigure 4. The pattern and composition of PC1. (**A**) Average contributions of 36 structural−related matrices to PC1**.**The contribution is measured as normalized absolute value of PCA coefficients. The dashed line indicates the expected average contributions (1/36). For details about SC-related matrices, please refer to eMethods. Although each structural feature largely contributes equally to PC1, weighted path length and binarized topological similarities (*i.e.*, cosine similarity and matching index), all of which heavily depend on the skeleton and strength of structure connectivity, are contributed slightly more, since their contributions are all ranked in the top 5. (**B**) The connectivity patterns of PC1. Interestingly, PC1 presents a prominent lobular-level modularized organization, that is, regions that belong to the same lobe are more connected. Therefore, we suggest PC1 reflects the general modularized organization of brain, which are mainly driven by shortest anatomical path (that is, the path with most strongly inter-connected nodes) and node similarity.

eFigure 5. The pattern and composition of PC2

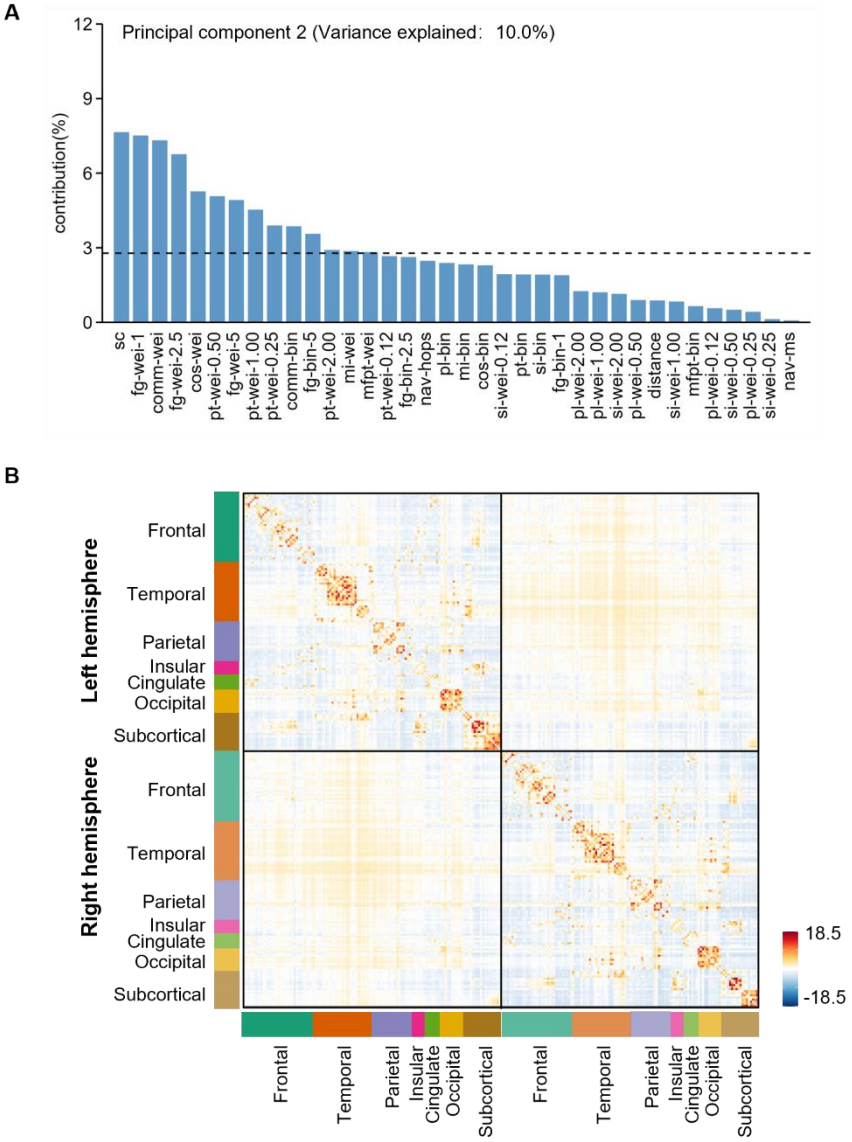

eFigure 5. The pattern and composition of PC2. (**A**) Average contributions of 36 structural−related matrices to PC2**.**The contribution is measured as normalized absolute value of PCA coefficients. The dashed line indicates the expected average contributions (1/36). For details about SC-related matrices, please refer to eMethods. The most contributed structural features are connectivity strength, communicability, and flow graph with short time range (*i.e.*, t = 1.0). (**B**) The connectivity patterns of PC2. Differing from PC1 significantly, PC2 presents a diagonal distribution, indicating a high locality connectivity. Accordingly, we consider PC2 mainly captures the local signal transmission pattern among brain regions dominated by direct anatomical connection.

eFigure 6. The pattern and composition of PC3

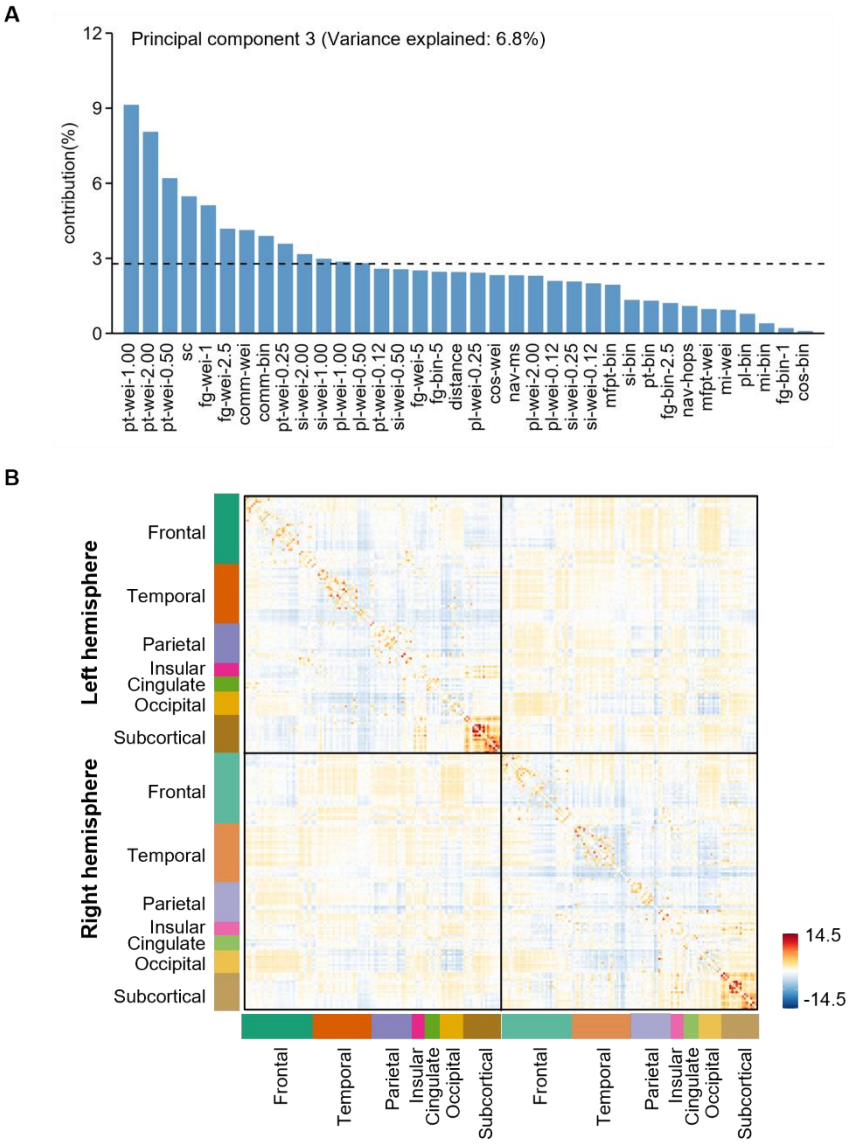

eFigure 6. The pattern and composition of PC3. (**A**) Average contributions of 36 structural−related matrices to PC3**.**The contribution is measured as normalized absolute value of PCA coefficients. The dashed line indicates the expected average contributions (1/36). For details about SC-related matrices, please refer to eMethods. The most contributed structural features for PC3 are path transitivity, which measure the density of local detours along the shortest paths[1]. (**B**) The connectivity patterns of PC3. PC3 is quite similar with PC2, with only subtle differences along the diagonal, *i.e.*, the weights between the source region and several near-most region is weaker than PC2. Therefore, we consider that PC3 captures another local information passing strategy driven by path transitivity, which may act as a compensation way for the local information communication relying on direct anatomical connections.

eFigure 7. The pattern and composition of PC4

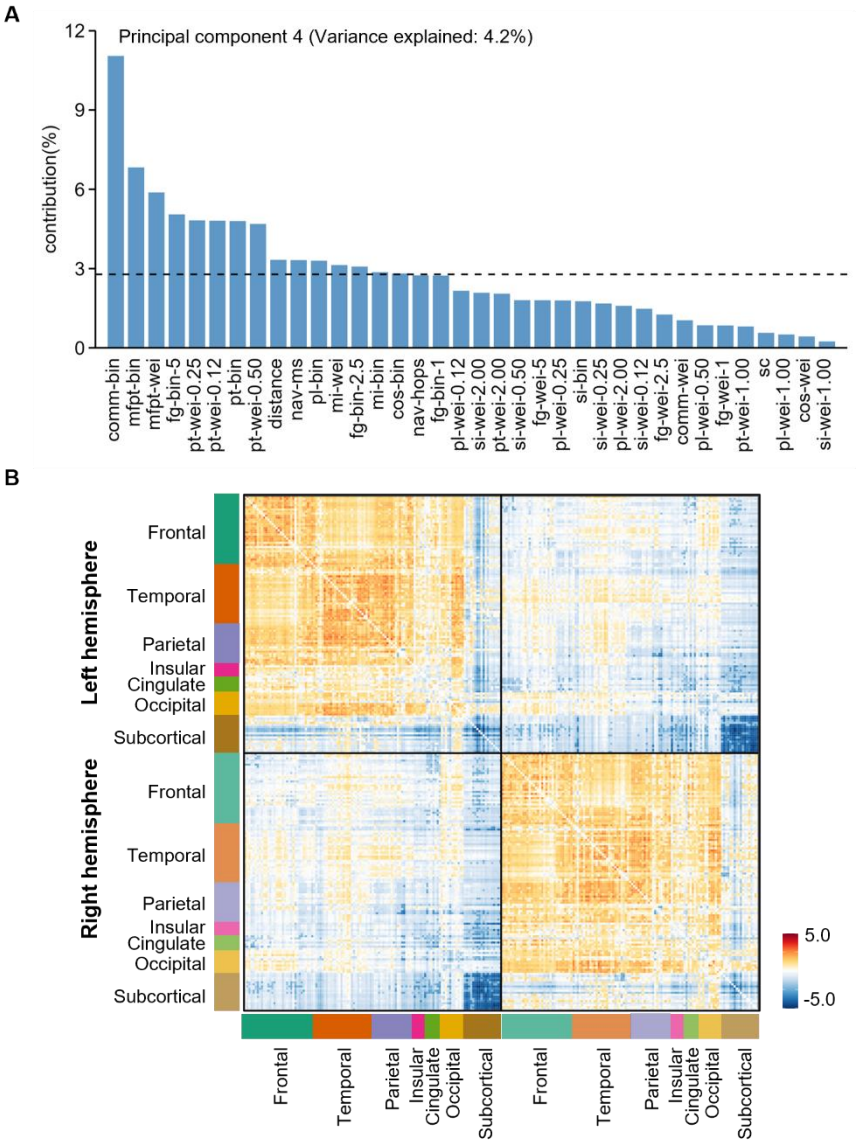

eFigure 7. The pattern and composition of PC4. (**A**) Average contributions of 36 structural−related matrices to PC4**.**The contribution is measured as normalized absolute value of PCA coefficients. The dashed line indicates the expected average contributions (1/36). For details about SC-related matrices, please refer to eMethods. The most contributed structural features for PC4 are communicability and mean first passage time based on the binarized structural connectivity. (**B**) The connectivity patterns of PC4. As PC4 largely relies on the binarized structural connectivity (*i.e.*, the information about the strength of direct anatomical connectivity is deprecated), the modularity within hemisphere and the local connectivity of each brain region are not prominent as PC1-3. However, we can find the weights of PC4 are differed among cortico-cortical connection, cortico-subcortical connection, and inter-hemisphere subcortical connection. Therefore, we consider that PC4 captures some patterns for long-range/inter-hemisphere macroscale communication in human brain, which may largely rely on subcortical structure to relay and modulate the incoming information.

eFigure 8. Average contributions of each PC for predicting regional FC in healthy subjects

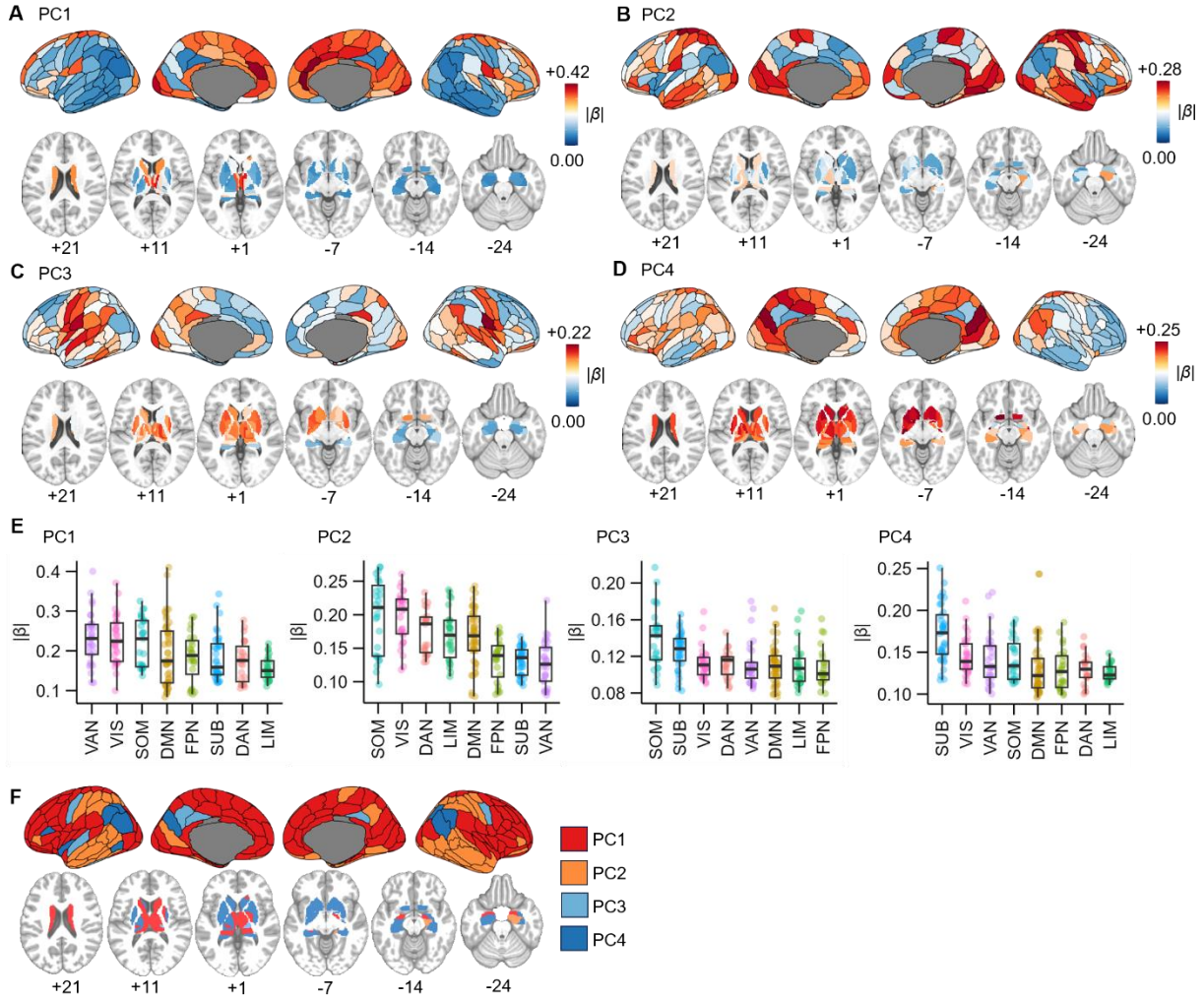

eFigure 8. Average contributions of each PC for predicting regional FC in healthy subjects. The contribution is measured as the absolute value of standardized beta weights in multilinear regression models which were built for fitting regional FC. Overall, the contributions of each PC for FC prediction are heterogenous. (**A**) Contributions of PC1 for predicting regional FC. PC1 contributes most for predicting the FC of frontal and superior parietal areas around the cortex middle line. (**B**) Contributions of PC2 for predicting regional FC. PC2 contributes relatively large for predicting the FC of paracentral areas and temporal areas. (**C**) Contributions of PC3 for predicting regional FC. PC3 contributes relatively large for predicting the FC of paracentral areas and insular areas. (**D**) Contributions of PC4 for predicting regional FC. PC4 contributes most for inferior parietal lobe and subcortical areas. (**E**) The distribution of contributions at the network level. Each point corresponds to a brain region. In each boxplot, the "box" indicates interquartile range (IQR), the horizontal bar indicated the median value, and the whiskers include points that are within 1.5×IQR of upper and lower bounds of the IQR. The contributions of the top 4 PCs are varied across brain networks (One-way ANOVA; PC1: $F_{(7,238)} = 5.56$, $p < 0.001$; PC2 : $F_{(7,238)} = 16.89$, $p < 0.001$; PC3 : $F_{(7,238)} = 7.06$, $p < 0.001$; PC4 : $F_{(7,238)} = 10.16$, $p < 0.001$). Specifically, PC1 contributes most for predicting FCs of regions in ventral attention network; PC2 and PC3 both contribute largely for predicting FCs of regions in somatomotor network; PC4 contributes largely for predicting FCs of subcortical regions. All PCs contribute largely for predicting FCs of regions in visual network. (**F**) The most contributive

PC for each brain region. The results suggest that the PC1 contributes the FC prediction largest for most brain regions, while other PCs have some region-specific contributions for FC prediction.

eFigure 9. Control analysis using matched healthy and MDD sample

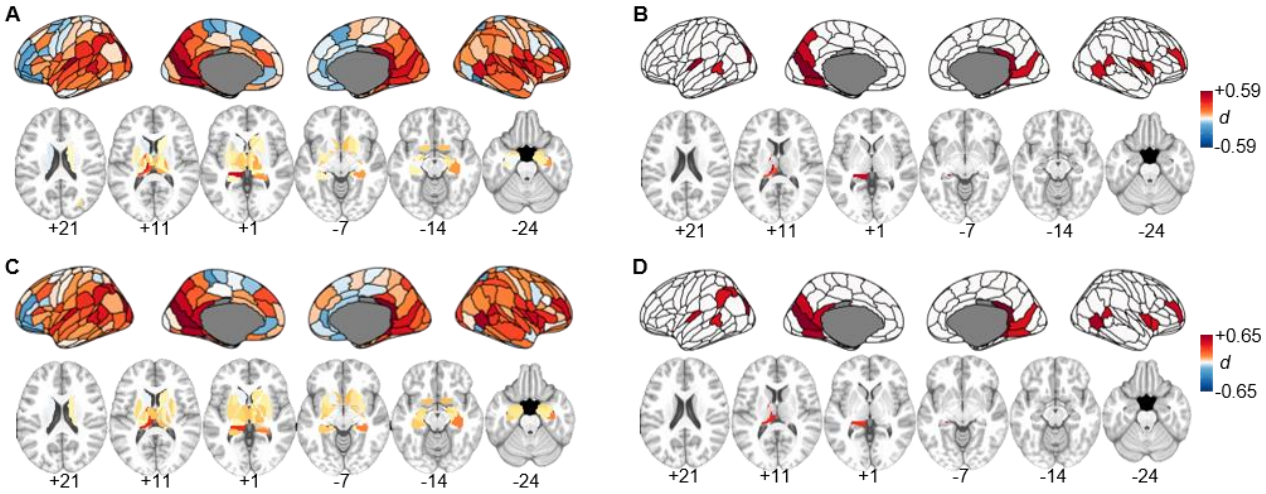

eFigure 9. SC−FC coupling differences between adolescent MDD and HCs after sample matching. (**A**) The differences of SC−FC coupling (measured as Cohen's *d*) between adolescent MDD (*n* = 168) and HCs (*n* = 101) at each brain region in the original cohort. (**B**) The SC−FC coupling of eighteen subregions show significant differences between adolescent MDD and HCs in the original cohort. (**C**) The differences of SC−FC coupling (measured as Cohen's *d*) between adolescent MDD (*n* = 101) and HCs (*n* = 101) at each brain region in the age−, gender− and BMI−matched sample. (D) The SC−FC coupling of twenty−two subregions show significant differences between adolescent MDD and HCs in the age−, gender− and BMI−matched sample.

eFigure 10. Subgroup differences in SC−FC coupling at each brain region

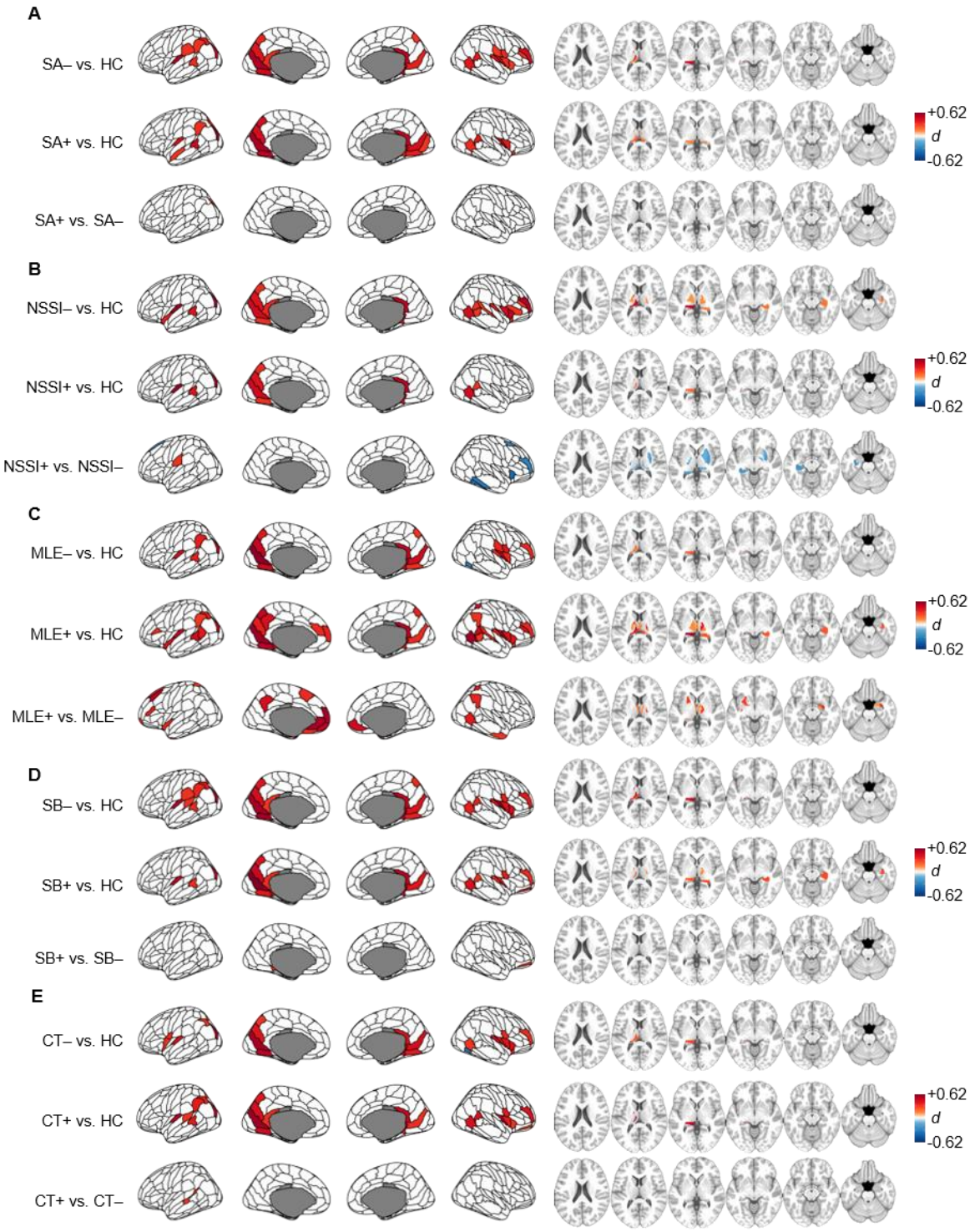

eFigure 10. Subgroup differences in SC−FC coupling. The Cohen's *d* is projected onto the brain, thresholding at $p < .05$. (**A**) Subgroup analysis of adolescent MDD with or without suicide attempt (SA+ and SA−). (**B**) Subgroup analysis of adolescent MDD with or without non−suicidal self−injury (NSSI+ and NSSI−). (**C**) Subgroup analysis of adolescent MDD with or without major life events (MLE+ and MLE−). (**D**) Subgroup analysis of adolescent MDD with or without

school bullying (SB+ and SB−). (**E**) Subgroup analysis of adolescent MDD with or without childhood trauma (CT+ and CT−).

eFigure 11. Regional SC−FC coupling differences among subgroups with different clinical characteristics

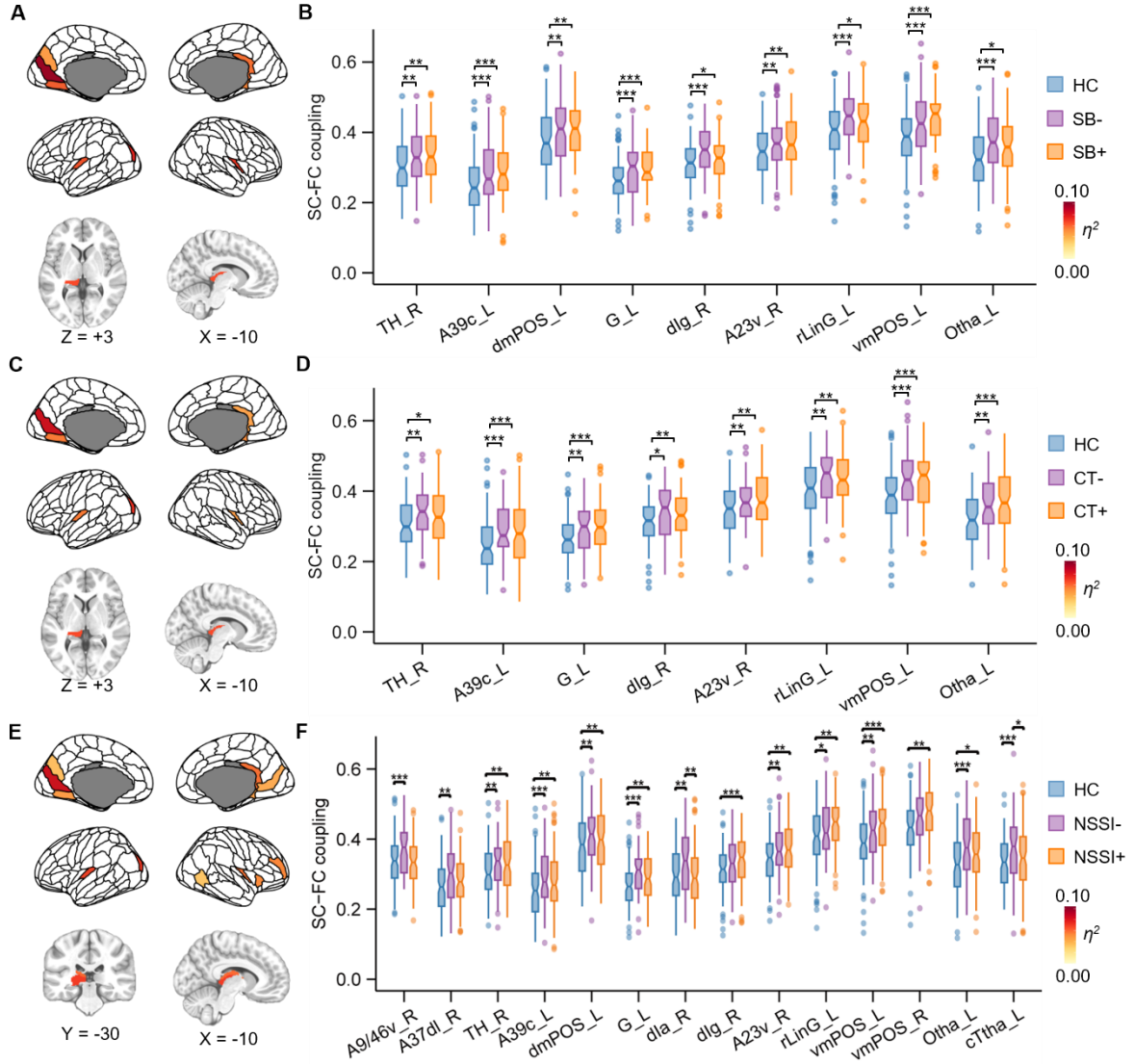

eFigure 11. Regional SC−FC coupling differences among subgroups with different clinical characteristics. In each boxplot, the "box" indicates interquartile range (IQR), the horizontal bar indicates the median value, and the whiskers include points that are within 1.5×IQR of upper and lower bounds of the IQR. (**A**) Regions with significant differences of SC−FC coupling among HCs, CT+ and CT−. Partial η^2 is mapped on the brain, thresholding at FDR−corrected $p < .05$. (**B**) *Post−hoc* comparisons of SC−FC coupling among HCs, CT+ and CT−. (**C**) Regions with significant differences of SC−FC coupling among HCs, SB+ and SB−. Partial η^2 is mapped on the brain, thresholding at FDR−corrected $p < .05$. (**D**) *Post−hoc* comparisons of SC−FC coupling among HCs, SB+ and SB−. (**E**) Regions with significant differences of SC-FC coupling among HCs, NSSI+ and NSSI−. (**F**) *Post-hoc* comparisons of SC-FC coupling among HCs, NSSI+ and NSSI−. Compared to HCs and NSSI+, NSSI− exhibited higher SC-FC coupling in subregions of right middle frontal gyrus (A9/46v), left thalamus (cTtha), right middle temporal gyrus (A37dl) and right insula (dIa).

eFigure 12. Sensitivity analysis of the effects owing to the medication status on the main group comparison results

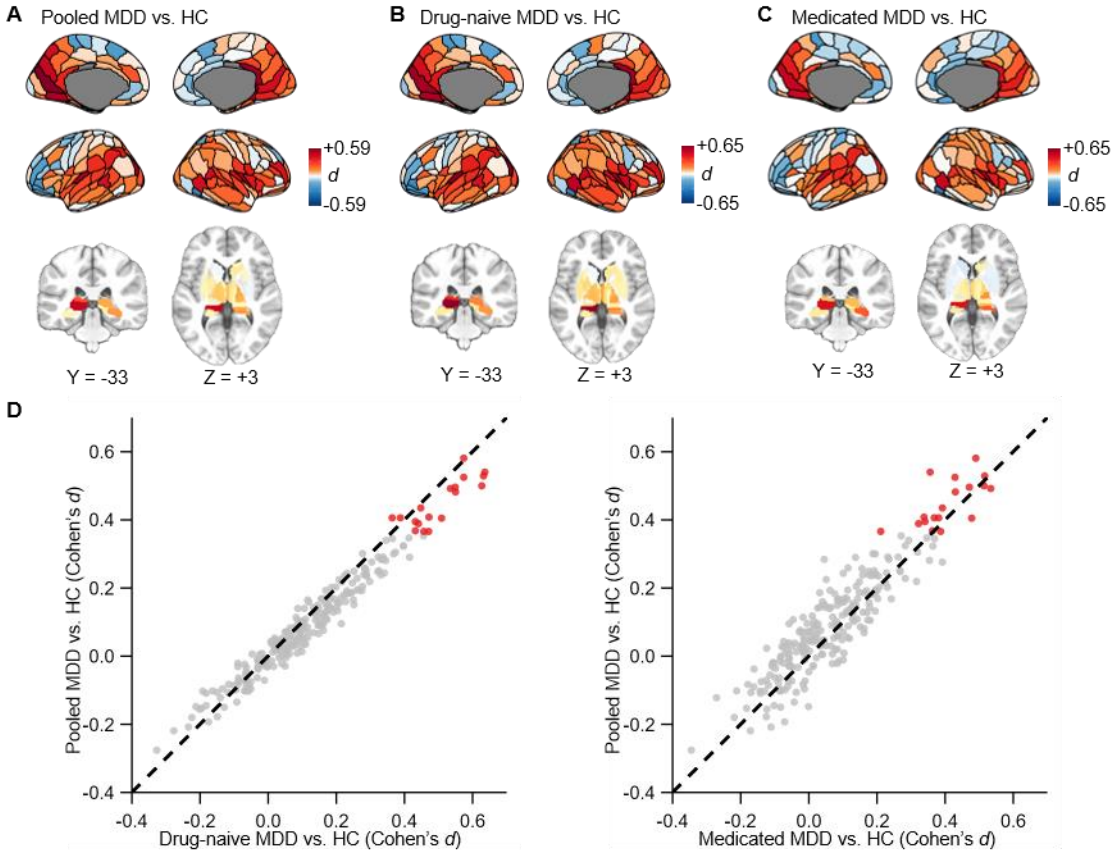

eFigure 12. Sensitivity analysis of the effects owing to the medication status on the main group comparison results. Confounders including age, sex, age^2, age × sex, age^2 × sex, BMI, total intracranial volume (ICV), and in−scanner head motion are regressed. (**A**) The differences of SC−FC coupling (measured as Cohen's *d*) between pooled adolescent MDD (*n* = 168) and HCs (*n* = 101). (**B**) The differences of SC−FC coupling (measured as Cohen's d) between drug−naïve adolescent MDD (*n* = 98) and HCs (*n* = 101). (**C**) The differences of SC−FC coupling (measured as Cohen's *d*) between medicated adolescent MDD (*n* = 70) and HCs (*n* = 101). (**D**) The SC−FC coupling alteration patterns are largely consensus regarding the medication−status.

eFigure 13. Sensitivity analysis of the effects owing to the gender on the main group comparison results

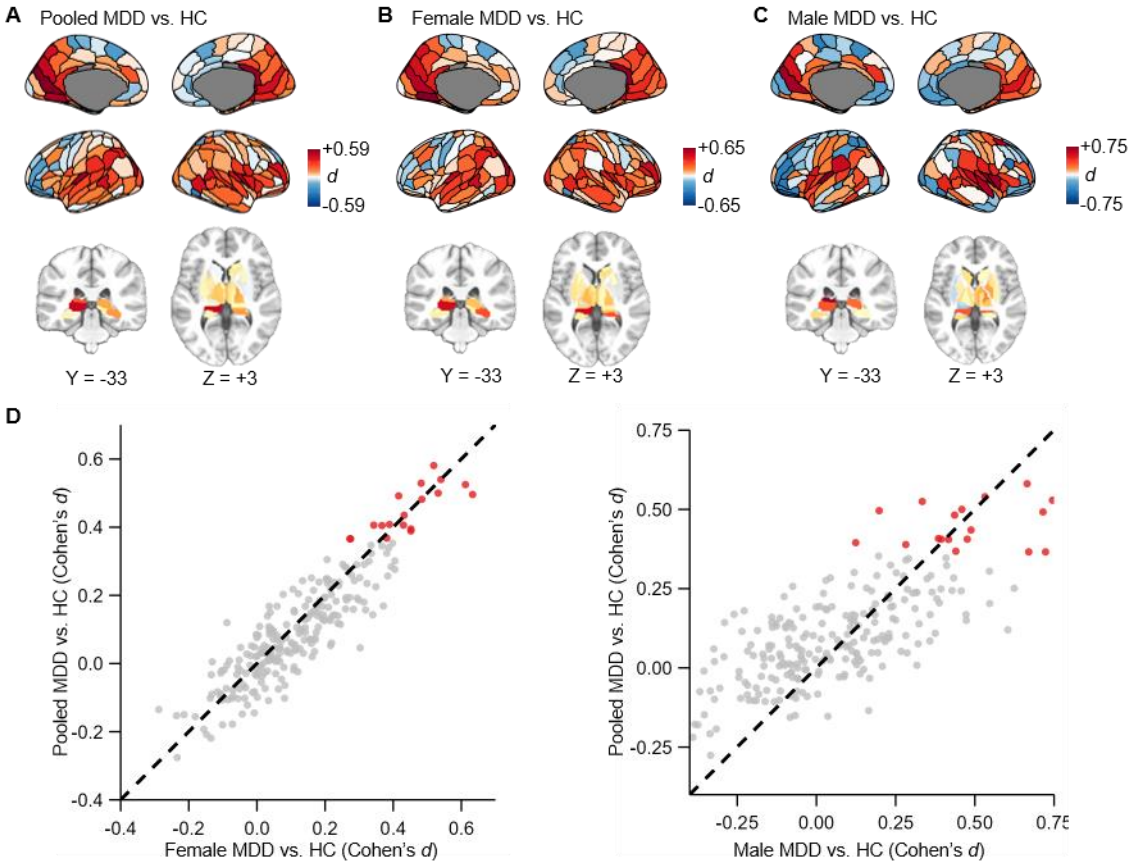

eFigure 13. Sensitivity analysis of the effects owing to the gender on the main group comparison results. Confounders including age, age^2, BMI, total intracranial volume (ICV), and in−scanner head motion are regressed. (**A**) The differences of SC−FC coupling (measured as Cohen's *d*) between pooled adolescent MDD (*n* = 168) and HCs (*n* = 101). (**B**) The differences of SC−FC coupling (measured as Cohen's *d*) between female adolescent MDD (*n* = 124) and female HCs (*n* = 61). (**C**) The differences of SC−FC coupling (measured as Cohen's *d*) between male adolescent MDD (*n* = 44) and male HCs (*n* = 40). (**D**) The SC−FC coupling alteration patterns are largely consensus across male and female subgroups.

eFigure 14. Sensitivity analysis of the effects owing to other behavioral and environmental factors on the main group comparison results

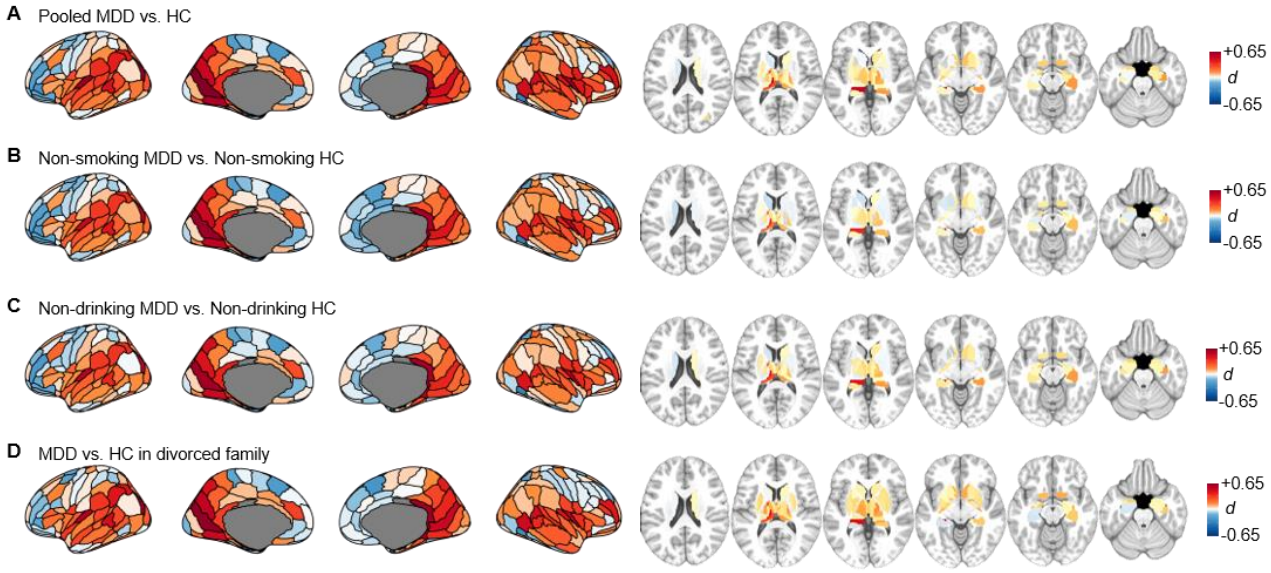

eFigure 14. Sensitivity analysis of the effects owing to other behavioral and environmental factors on the main group comparison results. Confounders including age, sex, age^2, age × sex, age^2 × sex, treatment history, BMI, total intracranial volume (ICV), and in−scanner head motion are regressed. (**A**) The differences of SC−FC coupling (measured as Cohen's *d*) between pooled adolescent MDD (*n* = 168) and HCs (*n* = 101). (**B**) The differences of SC−FC coupling (measured as Cohen's *d*) between non−smoking adolescent MDD (*n* = 151) and non−smoking HCs (*n* = 98). (**C**) The differences of SC−FC coupling (measured as Cohen's *d*) between non−drinking adolescent MDD (*n* = 148) and non−drinking HCs (*n* = 91). (**D**) The differences of SC−FC coupling (measured as Cohen's *d*) between adolescent MDD (*n* = 137) and HCs (*n* = 96) in non−divorced family.

eFigure 15. Distributions of the SC−FC coupling calculated by different SC−related matrices

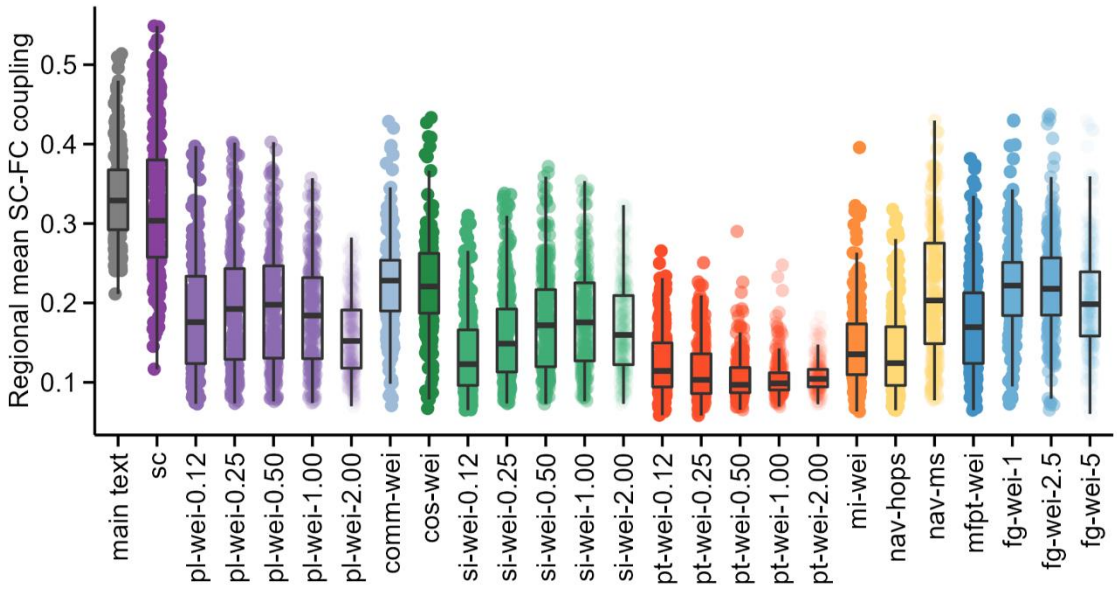

eFigure 15. Distributions of the SC−FC coupling calculated by different SC−related matrices. Each point represents the mean regional SC−FC coupling strength of a brain region across healthy participants. Compared with single predictor models, the SC−FC coupling strengths calculated in the main text were higher. For details about SC-related matrices, please refer to eMethods.

eFigure 16. Distributions of the SC−FC coupling calculated by selected combinations of SC−related matrices

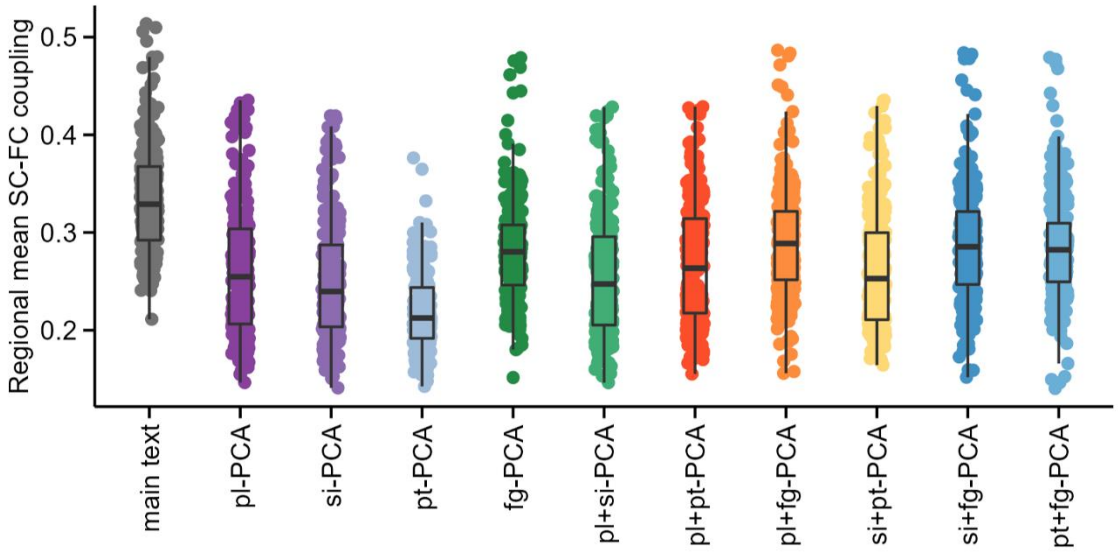

eFigure 16. Distributions of the SC−FC coupling calculated by selected combinations of SC−related matrices. In order to validate whether a subset of predictors could achieve comparable SC−FC coupling strength, we repeatedly calculated the SC−FC coupling strength based on ten selected combinations of predictors. Similarly, PCA was applied to generate three orthonormal bases which could collectively explain more than 80% of variance for all selected combinations. As the figure shown, the SC−FC coupling strengths calculated in the main text which utilized all predictors were higher than selected subsets of predictors. Each point represents the mean regional SC−FC coupling strength of a brain region across healthy participants. pl−PCA, PCA was performed on all path length−related matrices; si−PCA, PCA was performed on all search information−related matrices; pt−PCA, PCA was performed on all path transitivity−related matrices; fg−PCA, PCA was performed on all flow graph−related matrices; pl+si−PCA, PCA was performed on all path length−related matrices and search information−related matrices; pl+pt−PCA, PCA was performed on path length−related matrices and path transitivity−related matrices; si+pt−PCA, PCA was performed on search information−related matrices and path transitivity−related matrices; si+fg−PCA, PCA was performed on search information−related matrices flow grapth−related matrices; pt+fg−PCA, PCA was performed on path transitivity−related matrices and flow graph−related matrices.

eFigure 17. Correlations between the group differences of SC−FC coupling calculated based on all SC−related matrices and on single matrix

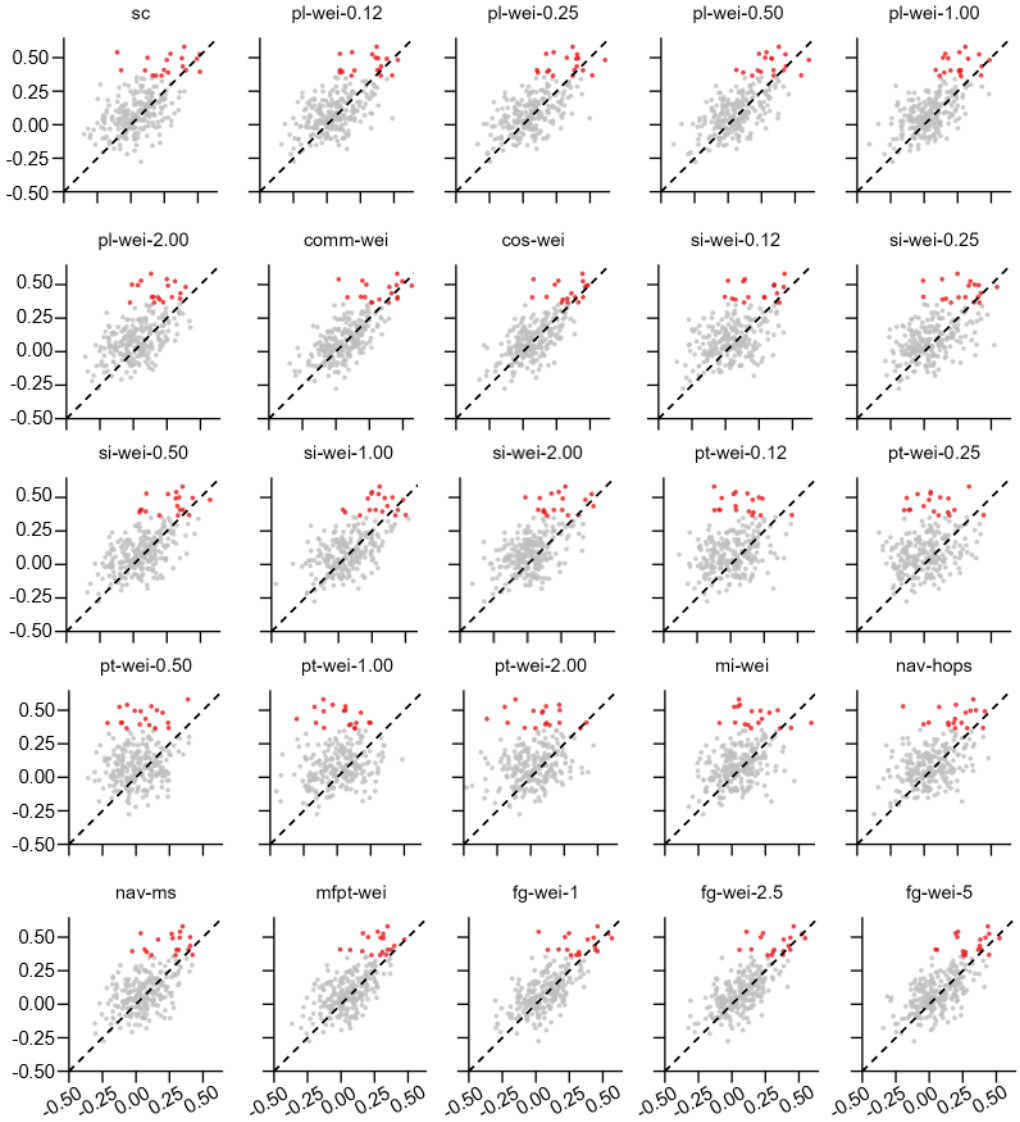

eFigure 17. Correlations between the group effect sizes of SC−FC coupling calculated based on all SC−related matrices and on single matrix. The red dots represent those abnormal subregions found in the main text. The distributions of the group differences of SC−FC coupling based on single predictor are largely in accordance with the results reported in the main text. Additionally, the SC−FC coupling calculated based on all predictors could achieve relatively higher effect sizes (the red dots tend to cluster at the right upside corner and above the diagonal line). For details about SC-related matrices, please refer to eMethods.

eFigure 18. Correlations between the group effect sizes of SC−FC coupling calculated based on all SC−related matrices and on selected subsets of matrices

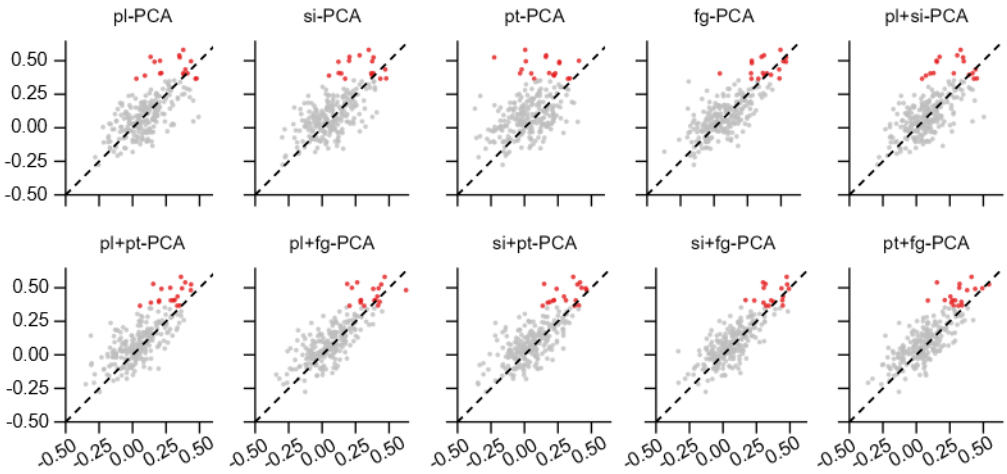

eFigure 18. Correlations between the group effect sizes of SC−FC coupling calculated based on all SC−related matrices and on selected subsets of matrices. The red dots represent those abnormal subregions found in the main text. The distributions of the group differences of SC−FC coupling based on selected subsets of predictors are largely in accordance with the results reported in the main text. Additionally, the SC−FC coupling calculated based on all predictors could achieve relatively higher effect sizes (the red dots tend to cluster at the right upside corner and above the diagonal line). pl−PCA, PCA was performed on all path length−related matrices; si−PCA, PCA was performed on all search information−related matrices; pt−PCA, PCA was performed on all path transitivity−related matrices; fg−PCA, PCA was performed on all flow graph−related matrices; pl+si−PCA, PCA was performed on all path length−related matrices and search information−related matrices; pl+pt−PCA, PCA was performed on path length−related matrices and path transitivity−related matrices; si+pt−PCA, PCA was performed on search information−related matrices and path transitivity−related matrices; si+fg−PCA, PCA was performed on search information−related matrices flow grapth−related matrices; pt+fg−PCA, PCA was performed on path transitivity−related matrices and flow graph−related matrices.

eFigure 19. The effect of different covariate sets on the group-differed SC-FC coupling patterns

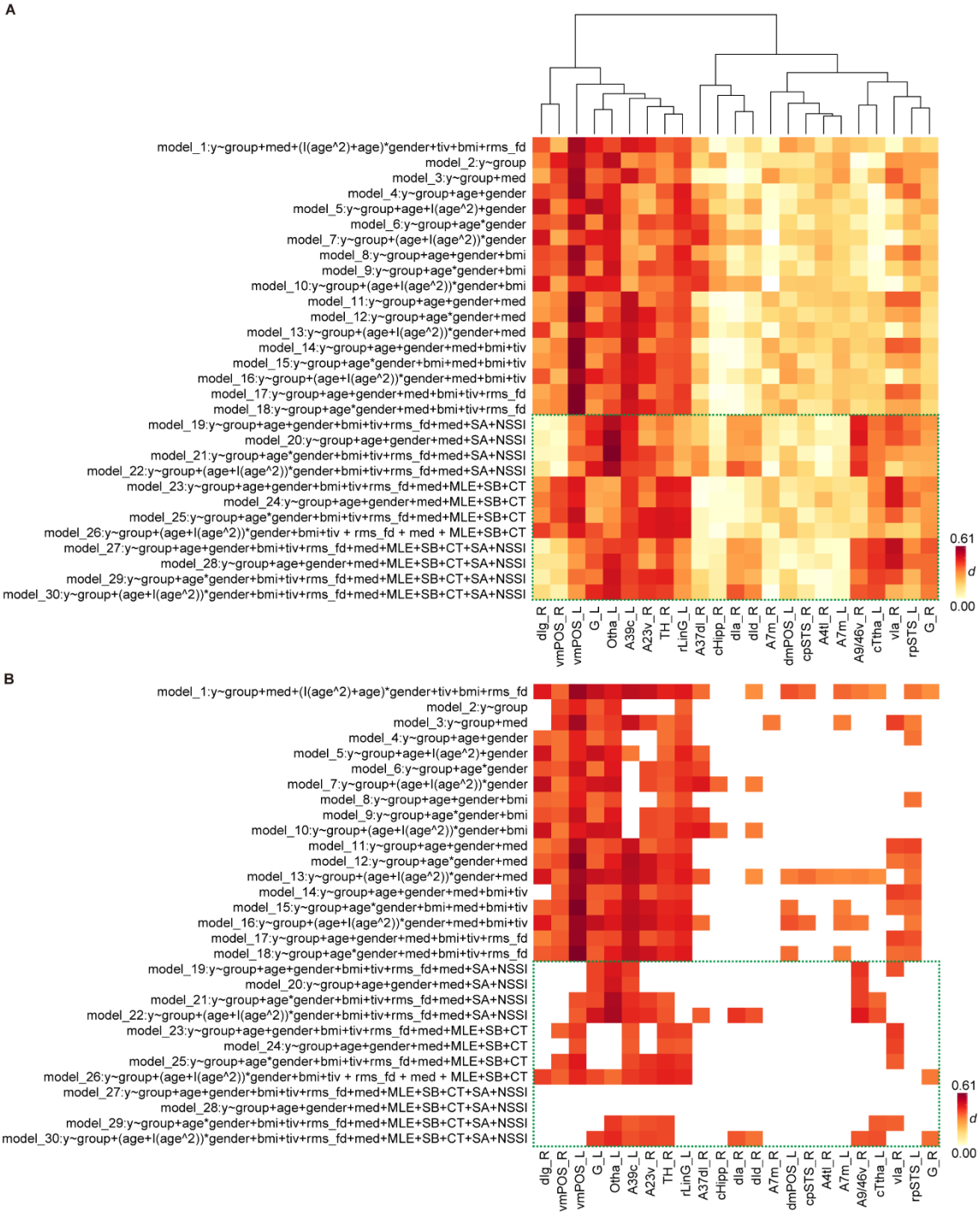

eFigure 19. The effect of different covariate sets on the group-differed SC-FC coupling patterns. Covariates sets were constructed by different combinations of demographic variables (*i.e.*, age, gender), procedural factors (*i.e.*, in-scanner head motion), anatomical variables (*i.e.*, BMI, ICV), clinical variable (*i.e.*, treatment history), and environmental/behavioral variables (*i.e.*, childhood trauma, suicide attempt, *etc.*). The green bounding box indicated the covariate sets including environmental/behavioral factos. (**A**) The effect sizes (Cohen's *d*) of brain regions with significant group differences (FDR corrected) obtained by different linear regression models. Only regions with significant group differences (FDR corrected) in least one model were presented. (**B**) The effect sizes (Cohen's *d*) of

brain regions with significant group differences (FDR corrected) in each linear regression model. Overall, SC-FC coupling increases in default mode network, insula and visual network in adolescent depression could be robustly identified in most models; and inclusions of environmental/behavioral variables will cancel some regions with significant group differences identified by other models.

eMethods

Assessment of childhood trauma

The Childhood Trauma Questionnaire (CTQ) is a 28-item assessment used to measure a history of childhood trauma. It includes five subscales that assess different types of traumas, such as emotional abuse, physical abuse, sexual abuse, emotional neglect, and physical neglect. Individuals with 1 or more subscales exceeded recommended cutoffs[2-4] were considered to have childhood trauma (cutoff scores: emotional abuse, 13; physical abuse, 10; sexual abuse, 8; emotional neglect, 15; physical neglect, 10).

Assessment of suicide attempt

The assessment of suicide attempt was based on the following six questions[5]:

1. *Have you wished you were dead or wished you could go to sleep and not wake up?*
2. *Have you had any actual thoughts of killing yourself?*
3. *Have you been thinking about how you might do this?*
4. *Have you had these thoughts and had some intention of acting on them?*
5. *Have you started to work out or worked out the details of how you would kill yourself? Do you intend to carry out this plan?*
6. *Have you ever done anything, started to do anything, or prepared to do anything to end your life?*

If the answers to questions 1 and 2 were both negative, the participants were considered to have no suicidal ideation. Otherwise, we continued to ask questions 3-6. If the participants have already taken some actions towards killing themselves (*i.e.*, the answer to question 6 was positive), they were considered to have suicide attempt. Otherwise, the participants were considered to only have suicidal ideation but without suicide attempt.

Assessment of non-suicidal self-injurious behavior

To assess non-suicidal self-injurious behavior, we asked participants if they had ever had an instance of directly and intentionally hurting themselves, such as scratching/cutting/pinching/biting/hitting themselves, pulling hair, *etc*. Participants who answered “No” were categorized as having no self-injurious behaviors. For those who answered “Yes”, we further inquired for their intention of the self-injurious behavior. Participants who confirmed engaging in self-injury without any intention to taking their own life (non-suicidal intention like stress relief, emotional improvement and seeking sympathy, *etc.*) were considered to have non-suicidal self-injurious behavior.

Assessment of major life events and school bullying

For assessment of major life events, we asked participants whether they had experienced a major stressful life event or not[6], such as life-threatening illnesses, the death or illness of a close friend or family member, parental divorce, financial difficulties, car accidents, and conflicts with romantic partners, *etc*. Participants who gave a confirmed answer were considered to have experienced major life events. Similarly for school bullying, we asked participants if they had experienced school bullying, such as verbal abuse, verbal threats, bodily injury, property damage, and sexual violence, or no school bullying experiences. Those who answered “Yes” were considered to have exposed to school bullying.

Image acquisition

Multimodal brain images were acquired using a Siemens Magnetom Skyra 3T scanner with a 32−channel head coil. Each participant was instructed to lie down and relax, to keep their eye closed and to stay awake and to avoid performing

specific cognitive task. The high resolution T1-weighted (T1w) structural images were acquired using magnetization−prepared rapid gradient−echo (MPRAGE) sequence with the following parameters: repetition time (TR) = 2000 ms, echo time (TE) = 2.56 ms, inversion time (TI) = 900 ms, flip angle = 9°, matrix size = 256 × 256, field of view (FOV) = 256 mm × 256 mm, slice thickness = 1 mm, slices per slab = 192, and voxel size was 1.0 mm × 1.0 mm × 1.0 mm. The resting−state fMRI was acquired using the gradient echo EPI sequence with following parameters: TR = 2000 ms, TE = 30 ms, flip angle = 90°, FOV = 220 mm× 220 mm, slice number = 36, and slice thickness = 3.0 mm. Totally 240 EPI volumes were acquired. The reconstructed voxel size was 3.4 mm × 3.4 mm × 3.0 mm, and the layer thickness was 3.0 mm. The parameters of diffusion−weighted MRI (DWI) were as follows: TR = 7000 ms, TE = 89.0 ms, acquisition matrix = 128 × 128, FOV = 256 mm × 256 mm, slice thickness = 3.0 mm, number of slices = 50, voxel resolution = 2.0 mm × 2.0 mm × 3.0 mm, flip angle = 90°, number of diffusion gradient directions = 64, b = 0 and 1000 s/mm2, number of excitations = 1.

Multimodal imaging data preprocessing

All available functional images and diffusion tensor images (DTI) were preprocessed using fMRIPrep 20.2.5 (RRID: SCR_016216)[7] and QSIPrep 0.14.3 (RRID: SCR_002502)[8], respectively. Both tools are based on Nipype 1.6.1 (RRID: SCR_002502)[9]. The following descriptions of fMRIPrep's and QSIPrep's preprocessing workflows are both based on boilerplate distributed with the software covered by 'no rights reserved' (CC0) license. Internal operations of fMRIPrep use Nilearn 0.6.2 [RRID: SCR_001362][10], ANTs 2.3.3 (RRID: SCR_004757), FSL 5.0.9 (RRID: SCR_002823), AFNI 20160207 (RRID: SCR_005927), and FreeSurfer 6.0.1 (RRID: SCR_001847). Internal operations of QSIPrep use Nilearn 0.8.1, ANTs 2.3.1, FSL 6.0.3, Dipy 1.3.0 (RRID: SCR_000029)[11], MRtrix 3.0 (RRID: SCR_006971)[12]. For more details of these two pipelines, please refer to the section corresponding to workflows in fMRIPrep's and QSIPrep's documentations.

Anatomical T1-weighted MRI preprocessing

T1w images were corrected for intensity non-uniformity (INU) using *N4BiasFieldCorrection*[13] distributed with ANTs and were used as T1-references. The T1w-reference was then skull-stripped with a Nipype implementation of the *antsBrainExtraction.sh* workflow, using the OASIS30ANTs as the target template. Brain tissue segmentation of cerebrospinal fluid (CSF), white-matter (WM) and gray-matter (GM) was performed on the brain-extracted T1w using *fast*[14]. Volume-based spatial normalization to the ICBM 152 Nonlinear Asymmetrical template version 2009c (MNI152NLin2009cAsym, RRID:SCR_008796)[15] was performed through nonlinear registration with *antsRegistration*[16], using brain-extracted versions of both T1w volume and the T1w template.

Resting state fMRI preprocessing

Functional images were motion corrected with respect to a BOLD reference volume (which had firstly been generated via a custom methodology of fMRIPrep) using FSL's *mcflirt*[17] and slice-time corrected using AFNI's *3dTshift*[18]. A deformation field to correct for susceptibility distortions was estimated using fMRIPrep's fieldmap-less approach[19,20]. Based on the estimated susceptibility distortion, a corrected EPI (echo-planar imaging) reference was calculated for a more accurate co-registration with the anatomical reference. The BOLD reference was then co-registered to the T1w image using FSL's *flirt*[21] with the boundary-based registration[22] cost-function. Co-registration was configured with nine degrees of freedom to account for distortions remaining in the BOLD reference. Motion correcting transformations, susceptibility-distortion-correcting warp, BOLD-to-T1w transformation and T1w-to-template (MNI152NLin2009cAsym) warp were concatenated and applied in a single step using *antsApplyTransforms* with Lanczos interpolation[23]. Several confounding time-series were calculated based on the preprocessed BOLD: framewise

displacement (FD), DVARS and three region-wise global signals. FD and DVARS were calculated for each functional run, both using their implementations in Nipype[24]. The three global signals were extracted within the CSF, the WM, and the whole-brain masks. The first ten volumes were discarded for signal stabilization.

DTI preprocessing

All DTI images were denoised with Marchenko-Pastur principal components analysis (MP-PCA) by MRtrix3's *dwidenoise*[25]. The B1 field inhomogeneity was then corrected using *dwibiascorrect* from MRtrix3 with the *N4* algorithm[13]. After B1 bias correction, the mean intensity of the DWI series was adjusted so all the mean intensity of the *b* = 0 images matched across each separate DWI scanning sequence. Head motion and eddy currents were further corrected using FSL's *eddy* with outlier replacement[26]. The *b* = 0 image from the preprocessed DWI data was registered to a skull-stripped, anterior commissure-posterior commissure (AC-PC) aligned T1w anatomical image. Finally, the DWI time-series were resampled into the AC-PC space with 2 mm isotropic voxels.

Diffusion model fitting

A ball−and−sticks diffusion model was fitted to each subject's resampled preprocessed DTI data using FSL's *bedpostx*, which runs Markov Chain Monte Carlo sampling to build up distributions on diffusion parameters at each voxel, and enables to model crossing fibers within each voxels[27]. After model fitting, probabilistic tractography was performed using FSL's *probtrackx2_gpu*, which respectively samples voxel-wise fiber orientation and diffusion parameter distributions to model anatomical trajectories between specified seed and target regions[27].

Seed and target regions for tractography

Seed and target regions were defined in native DTI space after co-registering the Brainnetome atlas to the resampled preprocessed *b* = 0 reference DWI image. The pipeline of defining the seed and target regions for probabilistic tractography was presented in **eFigure 2**. First, the preprocessed T1w anatomical images, brain tissue masks (GM, WM, CSF) and the brain atlas were all registered to the native DTI (AC-PC) space. Specifically, the preprocessed T1w images were registered to the resampled preprocessed DWI reference image (*b* = 0) through FSL's *flirt*, resulting a transformation matrix, *i.e.*, T1w2dwi.mat (**eFigure 2A**). Then, GM mask, WM mask, CSF mask were registered to native DWI space through FSL's *flirt* with T1w2dwi.mat as initialized transformation matrix, and the registered images were binarized at 0.5 to get the registered masks (**eFigure 2B**).

Second, the brain atlas was registered to the native DWI space via a two-step manner (**eFigure 2C**). Specifically, the brain atlas (in MNI space) was registered to native T1w space through *antsApplyTransforms*. Notably, the transforms (*i.e.*, MNI_to_t1w_xfm.h5) were automatically generated by the anatomical preprocessing workflow of fMRIprep. Then, FSL's *flirt* with initialized transformation matrix (T1w2dwi.mat) was applied to register the atlas generated from the former step to native DWI space. In both steps, the nearest neighborhood interpolation method was used.

Finally, the seed masks were defined in the native DTI space (**eFigure 2D**). For cortical regions, seed mask only included voxels in the ribbon along the gray-white boundary. For subcortical regions, seed mask included all voxels in each brain region defined by atlas. The gray-white boundary was defined by using *fslmaths –edge* function on the white matter segmentation mask in native DWI space, and the ribbon image was generated by dilating the gray-white matter boundary image by 2 mm. **eFigure 2H** illustrates the seed voxels of each brain regions defined by the Brainnetome atlas.

Each region was selected as a seed region and its connectivity strength to other 245 regions was calculated using probabilistic tractography. For each seed region, 2000×*n* streamlines were sampled, where *n* is the number of voxels in that region. Specifically, for cortical regions, only voxels in a ribbon along the gray-whiter boundary (**eFigure 2D**) were

selected as seed voxels, while all voxels in each subcortical region were selected as seed voxels due to its much smaller structure compared to cortical structures. For each streamline, the tracking parameters were as follows: step length = 0.5 mm, maximum steps = 2000, curvature threshold = 0.2 (*i.e.*, approximately correspond to 10° for maximum turning angle). Loop check was also enabled to avoid a streamline looped back itself. To increase the biological plausibility of white matter pathways reconstructed with probabilistic tractography, WM mask and CSF mask generated from fMRIprep's structural preprocessing workflow were also registered to native DWI spaced and were defined as waypoint mask and exclusion mask respectively, *i.e.*, only streamlines that passed through the WM mask would be considered valid and would be discarded if they entered cerebral-spinal fluid (**eFigure 2E-F**). Additionally, a superficial gray mask was generated by subtracting the seed mask from the GM mask and was defined as termination mask, *i.e.*, streamlines would be terminated as soon they entered superficial gray matter (**eFigure 2F**). This tractography process yielded a 246×246 weighted matrix, where each entry corresponded to the count of streamlines that passing through the seed and target region.

Image quality control

Data were assessed using visual reports generated from fMRIprep and QSIprep, and were also visually inspected for whole−brain field of view coverage. 3 participants were excluded due to failed preprocessing of DWI image. 4 participants were excluded due to incomplete MRI volume coverage or because of inadequate signal in several brain regions. Functional data with more than 25% of the frames exceeded 0.2 mm FD were considered to be contaminated by excessive head motion, resulting exclusions of 21 participants. Another 10 participants were excluded due to incomplete data collection, *e.g.*, lack of functional data or diffusion data.

SC-based communication models

As mentioned in the main text, the sparse structural connectivity matrix was transformed into 34 fully-weighted matrices based on a suite of communication strategies incorporating both centralized and decentralized processes, topological similarities, and spatial embeddings[28]. Each entry in these matrices described a putative functional linkage strength between the source and target regions. These 34 matrices included six path length matrices parameterized at different weight-to-cost transformations, two communicability matrices[29], two cosine similarity matrices, six search information matrices parameterized at different weight-to-cost transformations[1], six path transitivity matrices parameterized at different weight-to-cost transformations[1], two matching index matrices[30], two navigation matrices[31], two mean first passage time matrices[32], and six flow graphs parameterized at different time scales[33,34]. Additionally, Euclidean distance between two brain regions was also included as a predictor for functional connectivity. The followings presented the definition and calculation process of these matrices.

Path length. For weighted structural connectivity, the edge weight can be transformed to a cost. The path length l_{ij} can then be defined as the minimized total travel cost between brain region *i* and *j*. For binarized structural connectivity, the cost metric is identical to edge weight. In present study, the negative power of an edge weight w_{ij} was used for cost metric, *i.e.*, $c_{ij} = {w_{ij}}^{-\gamma}$, where $\gamma = 0.12, 0.25, 0.50, 1.00, 2.00$. Together, these matrices were denoted as *pl-bin* and *pl-wei-* followed by γ values.

Communicability. Communicability between a pair of brain regions is the weighted sum of the length of all possible walks[29]. For weighted structural connectivity, the communicability matrix is calculated as $C_{wei} = e^{A'}$, where A' is the normalized connectivity matrix, *i.e.*, $A' = D^{-1/2}AD^{1/2}$. For binarized network, the communicability is directly calculated as $C_{wei} = e^{A}$. These matrices were denoted as *comm-bin* and *comm-wei* in present study.

Cosine similarity. The cosine similarity is defined as the angle between two vectors, *i.e.*, $S_{ij} = w_i w_j / (\|w_i\| \|w_j\|)$. In present study, w_i and w_j corresponded to the structural connectivity profiles (the row of structural connectivity) of regions *i* and *j*. These metrices were denoted as *cos-wei* and *cos-bin* for weighted and binarized structural connectivity respectively.

Search information. Search information quantifies the information (in bits) required to access the shortest path linking a pair of brain regions[1]. For a given shortest path between brain region *s* and *t*, $\Omega_{s\to t} = \{s, i, j, \dots, k, t\}$ denotes the region sequence along the path, and $\pi_{s\to t} = \{w_{si}, w_{ij}, \dots, w_{kt}\}$ is the edge weight sequence along the path, the possibility of taking this path can be calculated as $p(\pi_{s\to t}) = p_{s\to i} \times p_{i\to j} \times \dots \times p_{k\to t}$, where $p_{i\to j} = \frac{A_{ij}}{\sum_j A_{ij}}$. Then, the search information SI_{st} between region *s* and *t* can then be calculated as $-\log_2 p(\pi_{s\to t})$. In present study, search information matrices were calculated based on path length matrices and were denoted as *si-bin* and *si-wei-* followed by corresponding γ values.

Matching index. Matching index quantifies the similarity between a pair of brain regions based on the overlap of their adjacent regions (excluding themselves) [1,30]. The adjacent region set N_i includes those regions with direct connections to region *i*, *i.e.*, $N_i = \{j | A_{ij} > 0\}$. The matching index can then be obtained by $MI_{ij} = \frac{|(N_i - \{j\}) \cap (N_j - \{i\})|}{|(N_i - \{j\}) \cup (N_j - \{i\})|}$. In present study, we denoted these matrices as *mi-bin* and *mi-wei* for binarized and weighted structural connectivity respectively.

Path transitivity. Path transitivity between the source region *s* and target region *t* measures the density of local detours available along the shortest path[1], and is calculated as $PT_{\pi(s\to t)} = \frac{2\sum_{i\in\Omega}\sum_{j\in\Omega} MI_{ij}}{|\Omega|(|\Omega|-1)}$. In present study, as path transitivity matrices were calculated based on path length matrices, these matrices were denoted as *pt-bin* and *pt-wei-* followed by corresponding γ values.

Navigation. Navigation describes an information routing strategy atop the network of anatomical pathways, *i.e.*, neural information always propagates from one region to another nearest region in some metric space. In present study, we calculated two matrices, *nav-ms* and *nav-hops*, based on navigation process atop the structural connectivity in Euclidean space. *nav-ms* corresponded to the total navigation length between each pair of brain regions, while *nav-hops* corresponded to the total number of hops between each pair of brain regions. Notably, navigation process doesn't guarantee a complete path from source region to target region. For incomplete navigation paths, the entries were filled with ∞.

Mean first passage time. Mean first passage time is defined as the expectation distance of a random walker travels from a source region to a target region. In present study, we denoted the mean first passage time as *mfpt-wei* and *mfpt-bin* for weighted and binarized structural connectivity matrix respectively.

Flow graphs. A flow graph[34] transforms an adjacency matrix of a network, A_{ij}, into a fully weighted adjacency matrix, $A(t)'_{ij}$, where each entry corresponds to the probabilistic flow of random walkers between regions *i* and *j* at time *t*. For a continuous-time random walkers with dynamics $\dot{p}_\iota = \sum_j L_{ij} p_j$, the corresponding flow graph is given by $A(t)'_{ij} = (e^{-tL})_{ij} s_j$, where the Laplacian operator $L_{ij} = \delta_{ij} - A_{ij}/s_j$, $s_j = \sum_i A_{ij}$. In present study, flow graphs were calculated based on both binarized (thresholding at 0) and weighted structural connectivity at different time scales, *i.e.*, *t* = 1, 2.5, 5. These matrices were denoted as *fg-bin-* and *fg-wei-* followed by parameter *t*.

Euclidean distance. In present study, Euclidean distance was calculated based on the centroid coordinates of brain regions defined by an atlas and was denoted as *distance*.

Matching procedure

In order to create a sample with balanced age, gender and BMI between healthy and depressive group, we used *R* package *MatchIt* [35] (*R* version 4.3.1, package version 4.5.4) to perform subset selection, which implements a wide range of matching methods for improving parametric statistical models. We used default parameters for the matching procedure, *i.e.*, a nearest neighbor matching on the propensity score estimated using logistic regression. The matching was based on age, gender and BMI, and ratio of healthy and depression subjects was 1:1.

Enrichment analysis via spin-based permutation testing

To evaluate whether the distribution of associations tended to be concentrated within specific brain cortical networks and lobar structure, enrichment analysis was conducted via spin−based permutation testing. The spin-based permutation test is a conservative statistical method with accounting for the different size of each network (lobe) and the spatial autocorrelation of brain structures (www.github.com/frantisekvasa/rotate_parcellation) [36,37]. Specifically, the proportion of brain cortical regions that survived the p thresholding ($p < .05$, uncorrected) of association analysis was calculated as the test statistics; the cortical statistical maps from association analysis were projected onto a sphere, which was rotated 5000 times to create a null distribution of the test statistics[38]. Networks (or lobes) were considered to have significant enrichment if the empirical test statistic was in the top 5% of the null distribution, *i.e.*, $p_{spin} < .05$.

eTable 1. The regions that defined in Brainnetome atlas at different levels

Lobe	Gyrus (Macro-anatomy level)	Left and Right Hemisphere (Subregion level)	Label ID.L	Label ID.R	Anatomical and modified Cyto-architectonic descriptions (Subregion level)	lh.MNI(X,Y,Z)	rh.MNI(X,Y,Z)
Frontal Lobe	SFG, Superior Frontal Gyrus	SFG_L(R)_7_1	1	2	*A8m, medial area 8*	−5 ,15, 54	7, 16, 54
		SFG_L(R)_7_2	3	4	*A8dl, dorsolateral area 8*	−18, 24, 53	22, 26, 51
		SFG_L(R)_7_3	5	6	*A9l, lateral area 9*	−11, 49, 40	13, 48, 40
		SFG_L(R)_7_4	7	8	*A6dl, dorsolateral area 6*	−18, −1, 65	20, 4, 64
		SFG_L(R)_7_5	9	10	*A6m, medial area 6*	−6, −5, 58	7, −4, 60
		SFG_L(R)_7_6	11	12	*A9m,medial area 9*	−5, 36, 38	6, 38, 35
		SFG_L(R)_7_7	13	14	*A10m, medial area 10*	−8, 56, 15	8, 58, 13
	MFG, Middle Frontal Gyrus	MFG_L(R)_7_1	15	16	*A9/46d, dorsal area 9/46*	−27, 43, 31	30, 37, 36
		MFG_L(R)_7_2	17	18	*IFJ, inferior frontal junction*	−42, 13, 36	42, 11, 39
		MFG_L(R)_7_3	19	20	*A46, area 46*	−28, 56, 12	28, 55, 17
		MFG_L(R)_7_4	21	22	*A9/46v, ventral area 9/46*	−41, 41, 16	42, 44, 14
		MFG_L(R)_7_5	23	24	*A8vl, ventrolateral area 8*	−33, 23, 45	42, 27, 39
		MFG_L(R)_7_6	25	26	*A6vl, ventrolateral area 6*	−32, 4, 55	34, 8, 54
		MFG_L(R)_7_7	27	28	*A10l, lateral area10*	−26, 60, −6	25, 61, −4
	IFG, Inferior Frontal Gyrus	IFG_L(R)_6_1	29	30	*A44d,dorsal area 44*	−46, 13, 24	45, 16, 25
		IFG_L(R)_6_2	31	32	*IFS, inferior frontal sulcus*	−47, 32, 14	48, 35, 13
		IFG_L(R)_6_3	33	34	*A45c, caudal area 45*	−53, 23, 11	54, 24, 12
		IFG_L(R)_6_4	35	36	*A45r, rostral area 45*	−49, 36, −3	51, 36, −1
		IFG_L(R)_6_5	37	38	*A44op, opercular area 44*	−39, 23, 4	42, 22, 3

		IFG_L(R)_6_6	39	40	*A44v, ventral area 44*	−52, 13, 6	54, 14, 11
	OrG, Orbital Gyrus	OrG_L(R)_6_1	41	42	*A14m, medial area 14*	−7, 54, −7	6, 47, −7
		OrG_L(R)_6_2	43	44	*A12/47o, orbital area 12/47*	−36, 33, −16	40, 39, −14
		OrG_L(R)_6_3	45	46	*A11l, lateral area 11*	−23, 38, −18	23, 36, −18
		OrG_L(R)_6_4	47	48	*A11m, medial area 11*	−6, 52, −19	6, 57, −16
		OrG_L(R)_6_5	49	50	*A13, area 13*	−10, 18, −19	9, 20, −19
		OrG_L(R)_6_6	51	52	*A12/47l, lateral area 12/47*	−41, 32, −9	42, 31, −9
	PrG, Precentral Gyrus	PrG_L(R)_6_1	53	54	*A4hf, area 4(head and face region)*	−49, −8, 39	55, −2, 33
		PrG_L(R)_6_2	55	56	*A6cdl, caudal dorsolateral area 6*	−32, −9, 58	33, −7, 57
		PrG_L(R)_6_3	57	58	*A4ul, area 4(upper limb region)*	−26, −25, 63	34, −19, 59
		PrG_L(R)_6_4	59	60	*A4t, area 4(trunk region)*	−13, −20, 73	15, −22, 71
		PrG_L(R)_6_5	61	62	*A4tl, area 4(tongue and larynx region)*	−52, 0, 8	54, 4, 9
		PrG_L(R)_6_6	63	64	*A6cvl, caudal ventrolateral area 6*	−49, 5, 30	51, 7, 30
	PCL, Paracentral Lobule	PCL_L(R)_2_1	65	66	*A1/2/3ll, area1/2/3 (lower limb region)*	−8, −38, 58	10, −34, 54
		PCL_L(R)_2_2	67	68	*A4ll, area 4, (lower limb region)*	−4, −23, 61	5, −21, 61
Temporal Lobe	STG, Superior Temporal Gyrus	STG_L(R)_6_1	69	70	*A38m, medial area 38*	−32, 14, −34	31, 15, −34
		STG_L(R)_6_2	71	72	*A41/42, area 41/42*	−54, −32, 12	54, −24, 11
		STG_L(R)_6_3	73	74	*TE1.0 and TE1.2*	−50, −11, 1	51, −4, −1
		STG_L(R)_6_4	75	76	*A22c, caudal area 22*	−62, −33, 7	66, −20, 6
		STG_L(R)_6_5	77	78	*A38l, lateral area 38*	−45, 11, −20	47, 12, −20
		STG_L(R)_6_6	79	80	*A22r, rostral area 22*	−55, −3, −10	56, −12, −5
	MTG, Middle Temporal Gyrus	MTG_L(R)_4_1	81	82	*A21c, caudal area 21*	−65, −30, −12	65, −29, −13
		MTG_L(R)_4_2	83	84	*A21r, rostral area 21*	−53, 2, −30	51, 6, −32

		MTG_L(R)_4_3	85	86	*A37dl, dorsolateral area37*	−59, −58, 4	60, −53, 3
		MTG_L(R)_4_4	87	88	*aSTS, anterior superior temporal sulcus*	−58, −20, −9	58, −16, −10
	ITG, Inferior Temporal Gyrus	ITG_L(R)_7_1	89	90	*A20iv, intermediate ventral area 20*	−45, −26, −27	46, −14, −33
		ITG_L(R)_7_2	91	92	*A37elv, extreme lateroventral area37*	−51, −57, −15	53, −52, −18
		ITG_L(R)_7_3	93	94	*A20r, rostral area 20*	−43, −2, −41	40, 0, −43
		ITG_L(R)_7_4	95	96	*A20il, intermediate lateral area 20*	−56, −16, −28	55, −11, −32
		ITG_L(R)_7_5	97	98	*A37vl, ventrolateral area 37*	−55, −60, −6	54, −57, −8
		ITG_L(R)_7_6	99	100	*A20cl, caudolateral of area 20*	−59, −42, −16	61, −40, −17
		ITG_L(R)_7_7	101	102	*A20cv, caudoventral of area 20*	−55, −31, −27	54, −31, −26
	FuG, Fusiform Gyrus	FuG_L(R)_3_1	103	104	*A20rv, rostroventral area 20*	−33, −16, −32	33, −15, −34
		FuG_L(R)_3_2	105	106	*A37mv, medioventral area37*	−31, −64, −14	31, −62, −14
		FuG_L(R)_3_3	107	108	*A37lv, lateroventral area37*	−42, −51, −17	43, −49, −19
	PhG, Parahippocampal Gyrus	PhG_L(R)_6_1	109	110	*A35/36r, rostral area 35/36*	−27, −7, −34	28, −8, −33
		PhG_L(R)_6_2	111	112	*A35/36c, caudal area 35/36*	−25, −25, −26	26, −23, −27
		PhG_L(R)_6_3	113	114	*TL, area TL (lateral PPHC, posterior parahippocampal gyrus)*	−28, −32, −18	30, −30, −18
		PhG_L(R)_6_4	115	116	*A28/34, area 28/34 (EC, entorhinal cortex)*	−19, −12, −30	19, −10, −30
		PhG_L(R)_6_5	117	118	*TI, area TI(temporal agranular insular cortex)*	−23, 2, −32	22, 1, −36
		PhG_L(R)_6_6	119	120	*TH, area TH (medial PPHC)*	−17, −39, −10	19, −36, −11
		pSTS_L(R)_2_1	121	122	*rpSTS, rostroposterior superior temporal sulcus*	−54, −40, 4	53, −37, 3

	pSTS, posterior Superior Temporal Sulcus	pSTS_L(R)_2_2	123	124	*cpSTS, caudoposterior superior temporal sulcus*	−52, −50, 11	57, −40, 12
Parietal Lobe	SPL, Superior Parietal Lobule	SPL_L(R)_5_1	125	126	*A7r, rostral area 7*	−16, −60, 63	19, −57, 65
		SPL_L(R)_5_2	127	128	*A7c, caudal area 7*	−15, −71, 52	19, −69, 54
		SPL_L(R)_5_3	129	130	*A5l, lateral area 5*	−33, −47, 50	35, −42, 54
		SPL_L(R)_5_4	131	132	*A7pc, postcentral area 7*	−22, −47, 65	23, −43, 67
		SPL_L(R)_5_5	133	134	*A7ip, intraparietal area 7(hIP3)*	−27, −59, 54	31, −54, 53
	IPL, Inferior Parietal Lobule	IPL_L(R)_6_1	135	136	*A39c, caudal area 39(PGp)*	−34, −80, 29	45, −71, 20
		IPL_L(R)_6_2	137	138	*A39rd, rostrodorsal area 39(Hip3)*	−38, −61, 46	39, −65, 44
		IPL_L(R)_6_3	139	140	*A40rd, rostrodorsal area 40(PFt)*	−51, −33, 42	47, −35, 45
		IPL_L(R)_6_4	141	142	*A40c, caudal area 40(PFm)*	−56, −49, 38	57, −44, 38
		IPL_L(R)_6_5	143	144	*A39rv, rostroventral area 39(PGa)*	−47, −65, 26	53, −54, 25
		IPL_L(R)_6_6	145	146	*A40rv, rostroventral area 40(PFop)*	−53, −31, 23	55, −26, 26
	Pcun, Precuneus	PCun_L(R)_4_1	147	148	*A7m, medial area 7(PEp)*	−5, −63, 51	6, −65, 51
		PCun_L(R)_4_2	149	150	*A5m, medial area 5(PEm)*	−8, −47, 57	7, −47, 58
		PCun_L(R)_4_3	151	152	*dmPOS, dorsomedial parietooccipital sulcus(PEr)*	−12, −67, 25	16, −64, 25
		PCun_L(R)_4_4	153	154	*A31, area 31 (Lc1)*	−6, −55, 34	6, −54, 35
	PoG, Postcentral Gyrus	PoG_L(R)_4_1	155	156	*A1/2/3ulhf, area 1/2/3(upper limb, head and face region)*	−50, −16, 43	50, −14, 44
		PoG_L(R)_4_2	157	158	*A1/2/3tonIa, area 1/2/3(tongue and larynx region)*	−56, −14, 16	56, −10, 15
		PoG_L(R)_4_3	159	160	*A2, area 2*	−46, −30, 50	48, −24, 48

		PoG_L(R)_4_4	161	162	*A1/2/3tru, area1/2/3(trunk region)*	−21, −35, 68	20, −33, 69
Insular Lobe	INS, Insular Gyrus	INS_L(R)_6_1	163	164	*G, hypergranular insula*	−36, −20, 10	37, −18, 8
		INS_L(R)_6_2	165	166	*vIa, ventral agranular insula*	−32, 14, −13	33, 14, −13
		INS_L(R)_6_3	167	168	*dIa, dorsal agranular insula*	−34, 18, 1	36, 18, 1
		INS_L(R)_6_4	169	170	*vId/vIg, ventral dysgranular and granular insula*	−38, −4, −9	39, −2, −9
		INS_L(R)_6_5	171	172	*dIg, dorsal granular insula*	−38, −8, 8	39, −7, 8
		INS_L(R)_6_6	173	174	*dId, dorsal dysgranular insula*	−38, 5, 5	38, 5, 5
Limbic Lobe	CG, Cingulate Gyrus	CG_L(R)_7_1	175	176	*A23d, dorsal area 23*	−4, −39, 31	4, −37, 32
		CG_L(R)_7_2	177	178	*A24rv, rostroventral area 24*	−3, 8, 25	5, 22, 12
		CG_L(R)_7_3	179	180	*A32p, pregenual area 32*	−6, 34, 21	5, 28, 27
		CG_L(R)_7_4	181	182	*A23v, ventral area 23*	−8, −47, 10	9, −44, 11
		CG_L(R)_7_5	183	184	*A24cd, caudodorsal area 24*	−5, 7, 37	4, 6, 38
		CG_L(R)_7_6	185	186	*A23c, caudal area 23*	−7, −23, 41	6, −20, 40
		CG_L(R)_7_7	187	188	*A32sg, subgenual area 32*	−4, 39, −2	5, 41, 6
Occipital Lobe	MVOcC, MedioVentral Occipital Cortex	MVOcC _L(R)_5_1	189	190	*cLinG, caudal lingual gyrus*	−11, −82, −11	10, −85, −9
		MVOcC _L(R)_5_2	191	192	*rCunG, rostral cuneus gyrus*	−5, −81, 10	7, −76, 11
		MVOcC _L(R)_5_3	193	194	*cCunG, caudal cuneus gyrus*	−6, −94, 1	8, −90, 12
		MVOcC _L(R)_5_4	195	196	*rLinG, rostral lingual gyrus*	−17, −60, −6	18, −60, −7
		MVOcC _L(R)_5_5	197	198	*vmPOS,ventromedial parietooccipital sulcus*	−13, −68, 12	15, −63, 12
	LOcC, lateral Occipital Cortex	LOcC_L(R)_4_1	199	200	*mOccG, middle occipital gyrus*	−31, −89, 11	34, −86, 11
		LOcC _L(R)_4_2	201	202	*V5/MT+, area V5/MT+*	−46, −74, 3	48, −70, −1
		LOcC _L(R)_4_3	203	204	*OPC, occipital polar cortex*	−18, −99, 2	22, −97, 4

		LOcC_L(R)_4_4	205	206	*iOccG, inferior occipital gyrus*	−30, −88, −12	32, −85, −12
		LOcC _L(R)_2_1	207	208	*msOccG, medial superior occipital gyrus*	−11, −88, 31	16, −85, 34
		LOcC _L(R)_2_2	209	210	*lsOccG, lateral superior occipital gyrus*	−22, −77, 36	29, −75, 36
Subcortical Nuclei	Amyg, Amygdala	Amyg_L(R)_2_1	211	212	*mAmyg, medial amygdala*	−19, −2, −20	19, −2, −19
		Amyg_L(R)_2_2	213	214	*lAmyg, lateral amygdala*	−27, −4, −20	28, −3, −20
	Hipp, Hippocampus	Hipp_L(R)_2_1	215	216	*rHipp, rostral hippocampus*	−22, −14, −19	22, −12, −20
		Hipp_L(R)_2_2	217	218	*cHipp, caudal hippocampus*	−28, −30, −10	29, −27, −10
	BG, Basal Ganglia	BG_L(R)_6_1	219	220	*vCa, ventral caudate*	−12, 14, 0	15, 14, −2
		BG_L(R)_6_2	221	222	*GP, globus pallidus*	−22, −2, 4	22, −2, 3
		BG_L(R)_6_3	223	224	*NAC, nucleus accumbens*	−17, 3, −9	15, 8, −9
		BG_L(R)_6_4	225	226	*vmPu, ventromedial putamen*	−23, 7, −4	22, 8, −1
		BG_L(R)_6_5	227	228	*dCa, dorsal caudate*	−14, 2, 16	14, 5, 14
		BG_L(R)_6_6	229	230	*dlPu, dorsolateral putamen*	−28, −5, 2	29, −3, 1
	Tha, Thalamus	Tha_L(R)_8_1	231	232	*mPFtha, medial pre-frontal thalamus*	−7, −12, 5	7, −11, 6
		Tha_L(R)_8_2	233	234	*mPMtha, pre-motor thalamus*	−18, −13, 3	12, −14, 1
		Tha_L(R)_8_3	235	236	*Stha, sensory thalamus*	−18, −23, 4	18, −22, 3
		Tha_L(R)_8_4	237	238	*rTtha, rostral temporal thalamus*	−7, −14, 7	3, −13, 5
		Tha_L(R)_8_5	239	240	*PPtha, posterior parietal thalamus*	−16, −24, 6	15, −25, 6
		Tha_L(R)_8_6	241	242	*Otha, occipital thalamus*	−15, −28, 4	13, −27, 8
		Tha_L(R)_8_7	243	244	*cTtha, caudal temporal thalamus*	−12, −22, 13	10, −14, 14
		Tha_L(R)_8_8	245	246	*lPFtha, lateral pre-frontal thalamus*	−11, −14, 2	13, −16, 7

eTable 2. Statistical analysis of sociodemographic and clinical characteristics among heathy controls without childhood trauma (HC), adolescent MDD with and without childhood trauma (CT+/CT−). Kruskal-Wallis's test (*H*) was used to analysis group differences of age, body mass index (BMI), and clinical scales. χ^2 test was performed to analyze interactions between groups and categorical variables when each count ≥ 5, *i.e.*, gender, environmental variables, behavioral variables, and medication status; otherwise, Fisher's exact test was performed. MAD, median absolute deviation; NA, not applicable.

Variables	HCs (*n* = 91)	CT− (*n* = 62)	CT+ (*n* = 106)	Statistical analysis	*P* value
Demographic variables					
Age (median [MAD], years)	14.5 [2.0]	16.2 [1.0]	16.1 [1.4]	$H_{2,256}$ = 9.761	.008
Gender (Male/Female)	35/56	22/40	22/84	χ_2^2 = 8.196	.017
BMI (median [MAD], kg/m^2)	20.3 [2.4]	20.1 [2.2]	20.1 [1.9]	$H_{2,256}$ = 0.536	.765
Environmental variables					
Parents divorced (Yes/No)	5/86	11/51	20/86	χ_2^2 = 8.323	.016
School bullying (Yes/No)	5/86	14/48	56/50	χ_2^2 = 54.942	< .001
Major life events (Yes/No)	13/78	14/48	47/59	χ_2^2 = 23.105	< .001
CTQ (median [MAD])	33.0 [4.0]	34.5 [3.5]	46.5 [5.5]	$H_{2,256}$ = 150.049	< .001
Behavioral variables					
Suicide attempt (Yes/No)	0/91	14/48	41/65	NA	< .001
Non-suicidal self-injury (Yes/No)	2/89	32/30	71/35	NA	< .001
Smoking (Yes/No)	3/88	2/60	15/91	NA	.006
Drinking (Yes/No)	7/84	5/57	15/91	χ_2^2 = 2.674	.263
Clinical variables					
HAMA (median [MAD])	NA	12.5 [4.5]	16.0 [5.0]	$H_{1,166}$ = 5.875	.015
HAMD-17 (median [MAD])	NA	12.5 [4.0]	19.0 [4.0]	$H_{1,166}$ = 4.419	.036
Medication history (Yes/No)	NA	26/36	44/62	χ_1^2 = 0.003	.957

eTable 3. Statistical analysis of sociodemographic and clinical characteristics among heathy controls without school bullying (HC), adolescent MDD with and without school bullying (SB+/SB−). Kruskal-Wallis's test (*H*) was used to analysis group differences of age, body mass index (BMI), and clinical scales. χ^2 test was performed to analyze interactions between groups and categorical variables when each count ≥ 5, *i.e.*, gender, environmental variables, behavioral variables, and medication status; otherwise, Fisher's exact test was performed. MAD, median absolute deviation; NA, not applicable.

Variables	**HCs (*n* = 93)**	**SB− (*n* = 98)**	**SB+ (*n* = 70)**	**Statistical analysis**	***P* value**
Demographic variables					
Age (median [MAD], years)	14.5 [1.8]	16.2 [0.9]	16.1 [1.4]	$H_{2,258}$ = 12.346	.002
Gender (Male/Female)	37/56	29/69	15/55	χ_2^2 = 6.440	.040
BMI (median [MAD], kg/m^2)	20.3 [2.4]	19.7 [2.3]	20.3 [1.7]	$H_{2,258}$ = 3.214	.201
Environmental variables					
Parents divorced (Yes/No)	3/90	13/85	18/52	NA	< .001
Childhood trauma (Yes/No)	7/86	50/48	56/14	χ_2^2 = 89.260	< .001
Major life events (Yes/No)	11/82	28/70	33/37	χ_2^2 = 25.011	< .001
CTQ (median [MAD])	34.0 [4.0]	39.0 [6.0]	45.0 [7.0]	$H_{2,258}$ = 60.455	< .001
Behavioral variables					
Suicide attempt (Yes/No)	0/93	28/70	27/43	NA	< .001
Non-suicidal self-injury (Yes/No)	1/92	54/44	49/21	NA	< .001
Smoking (Yes/No)	3/90	8/90	9/61	NA	< .071
Drinking (Yes/No)	7/86	10/88	10/60	χ_2^2 = 1.971	.037
Clinical variables					
HAMA (median [MAD])	NA	13.0 [4.0]	16.0 [5.0]	$H_{1,166}$ = 4.060	.044
HAMD-17 (median [MAD])	NA	13.0 [4.0]	19.0 [4.0]	$H_{1,166}$ = 1.172	.279
Medication history (Yes/No)	NA	42/56	28/42	χ_1^2 = 0.137	.711

eTable 4. Statistical analysis of sociodemographic and clinical characteristics among heathy controls without major life events (HC), adolescent MDD with and without major life events (MLE+/MLE−). Kruskal-Wallis's test (*H*) was used to analysis group differences of age, body mass index (BMI), and clinical scales. χ^2 test was performed to analyze interactions between groups and categorical variables when each count ≥ 5, *i.e.*, gender, environmental variables, behavioral variables, and medication status; otherwise, Fisher's exact test was performed. MAD, median absolute deviation; NA, not applicable.

Variables	HCs (*n* = 87)	MLE− (*n* = 107)	MLE+ (*n* = 61)	Statistical analysis	*P* value
Demographic variables					
Age (median [MAD], years)	14.8 [2.0]	16.1 [1.3]	16.3 [1.2]	$H_{2,252}$ = 10.637	.005
Gender (Male/Female)	33/54	27/80	17/44	χ^2_2 = 3.876	.144
BMI (median [MAD], kg/m^2)	20.0 [2.3]	20.0 [2.4]	20.2 [1.5]	$H_{2,252}$ = 2.054	.358
Environmental variables					
Parents divorced (Yes/No)	3/84	12/95	19/42	NA	< .001
Childhood trauma (Yes/No)	9/78	59/48	47/14	χ^2_2 = 71.948	< .001
School bullying (Yes/No)	5/82	37/70	33/28	χ^2_2 = 42.749	< .001
CTQ (median [MAD])	34.0 [4.0]	40.0 [5.0]	45.0 [7.0]	$H_{2,252}$ = 51.059	< .001
Behavioral variables					
Suicide attempt (Yes/No)	0/87	33/74	39/22	NA	< .001
Non-suicidal self-injury (Yes/No)	1/86	65/42	38/23	NA	< .001
Smoking (Yes/No)	2/85	6/101	11/50	NA	.001
Drinking (Yes/No)	6/81	10/97	10/51	χ^2_2 = 3.678	.159
Clinical variables					
HAMA (median [MAD])	NA	15.0 [5.0]	14.0 [4.0]	$H_{1,166}$ = 1.005	.0316
HAMD-17 (median [MAD])	NA	15.0 [5.0]	17.0 [3.0]	$H_{1,166}$ = 0.915	.339
Medication history (Yes/No)	NA	43/64	27/34	χ^2_1 = 0.266	.606

eTable 5. Statistical analysis of sociodemographic and clinical characteristics among heathy controls without suicidal attempt (HC), adolescent MDD with and without suicide attempt (SA+/SA−). Kruskal-Wallis's test (*H*) was used to analysis group differences of age, body mass index (BMI), and clinical scales. χ^2 test was performed to analyze interactions between groups and categorical variables when each count ≥ 5, *i.e.*, gender, environmental variables, behavioral variables, and medication status; otherwise, Fisher's exact test was performed. MAD, median absolute deviation. NA, not applicable.

Variables	HCs (*n* = 101)	SA− (*n* = 113)	SA+ (*n* = 55)	Statistical analysis	*P* value
Demographic variables					
Age (median [MAD], years)	14.8 [2.0]	16.3 [1.2]	16.0 [1.1]	$H_{2,266}$ = 11.021	.004
Gender (Male/Female)	40/61	36/77	8/47	χ^2_2 = 10.448	.005
BMI (median [MAD], kg/m^2)	20.3 [2.4]	20.1 [2.2]	19.8 [1.6]	$H_{2,266}$ = 1.182	.554
Environmental variables					
Parents divorced (Yes/No)	5/96	16/97	15/40	χ^2_2 = 15.408	< .001
Childhood trauma (Yes/No)	8/93	43/70	27/28	χ^2_2 = 37.079	< .001
School bullying (Yes/No)	10/91	65/48	41/14	χ^2_2 = 77.143	< .001
Major life events (Yes/No)	14/87	39/74	22/33	χ^2_2 = 16.362	< .001
CTQ (median [MAD])	34.0 [4.0]	41.0 [6.0]	44.0 [7.0]	$H_{2,256}$ = 52.191	< .001
Behavioral variables					
Non-suicidal self-injury (Yes/No)	2/99	59/54	44/11	NA	< .001
Smoking (Yes/No)	3/98	9/104	8/47	NA	< .001
Drinking (Yes/No)	10/91	9/104	11/44	χ^2_2 = 5.664	.059
Clinical variables					
HAMA (median [MAD])	NA	13.0 [4.0]	18.0 [5.0]	$H_{1,166}$ = 11.534	< .001
HAMD-17 (median [MAD])	NA	13.0 [3.0]	21.0 [4.0]	$H_{1,166}$ = 15.918	< .001
Medication history (Yes/No)	NA	45/68	25/30	χ^2_1 = 0.483	.487

eTable 6. Statistical analysis of sociodemographic and clinical characteristics among heathy controls without non−suicidal self−injurious behavior (HC), adolescent MDD with and without non−suicidal self−injurious behavior (NSSI+/NSSI−). Kruskal-Wallis's test (*H*) was used to analysis group differences of age, body mass index (BMI), and clinical scales. χ^2 test was performed to analyze interactions between groups and categorical variables when each count ≥ 5, *i.e.*, gender, environmental variables, behavioral variables, and medication status; otherwise, Fisher's exact test was performed. MAD, median absolute deviation; NA, not applicable

Variables	**HCs (*n* = 99)**	**NSSI− (*n* = 65)**	**NSSI+ (*n* = 103)**	**Statistical analysis**	***P* value**
Demographic variables					
Age (median [MAD], years)	14.8 [2.0]	16.5 [1.0]	15.9 [1.2]	$H_{2,264}$ = 14.750	< .001
Gender (Male/Female)	40/59	29/36	15/88	χ^2_2 = 22.527	< .001
BMI (median [MAD], kg/m^2)	20.3 [2.4]	20.1 [1.7]	20.1 [2.5]	$H_{2,264}$ = 1.116	.572
Environmental variables					
Parents divorced (Yes/No)	5/94	11/54	20/83	χ^2_2 = 9.804	.007
Childhood trauma (Yes/No)	10/89	35/30	71/32	χ^2_2 = 74.891	< .001
School bullying (Yes/No)	7/92	21/44	49/54	χ^2_2 = 40.855	< .001
Major life events (Yes/No)	13/86	23/42	38/65	χ^2_2 = 16.750	< .001
CTQ (median [MAD])	34.0 [4.0]	40.0 [6.0]	43.0 [6.0]	$H_{2,264}$ = 49.664	< .001
Behavioral variables					
Suicide attempt (Yes/No)	0/99	11/54	44/59	NA	< .001
Smoking (Yes/No)	3/96	6/59	11/92	NA	< .001
Drinking (Yes/No)	10/89	5/60	15/88	χ^2_2 = 2.090	.352
Clinical variables					
HAMA (median [MAD])	NA	12.0 [4.0]	16.0 [5.0]	$H_{1,166}$ = 8.545	.003
HAMD-17 (median [MAD])	NA	12.0 [4.0]	19.0 [4.0]	$H_{1,166}$ = 16.771	< .001
Medication history (Yes/No)	NA	22/43	48/55	χ^2_1 = 2.668	.102

eTable 7. Statistical analysis of differences between MDD and HCs. For abbreviations of anatomy and brain regions, please refer to eTable 1. Both FDR corrected p-value (P_{adj}) and original p-value (P) are provided.

ID	Subregion	Anatomy	*T*	Cohen's *d*	95% CI	*P*	P_{adj}
22	A9/46v_R	MFG	3.125	0.389	[0.142, 0.635]	.002	.032
86	A37dl_R	MTG	3.249	0.405	[0.158, 0.651]	.001	.025
120	TH_R	PhG	3.868	0.482	[0.234, 0.729]	< .001	.004
121	rpSTS_L	pSTS	3.169	0.395	[0.148, 0.641]	.002	.030
124	cpSTS_R	pSTS	3.273	0.408	[0.161, 0.654]	.001	.025
135	A39c_L	IPL	4.339	0.540	[0.291, 0.788]	< .001	.002
147	A7m_L	Pcun	3.259	0.406	[0.159, 0.652]	.001	.025
151	dmPOS_L	Pcun	3.495	0.435	[0.188, 0.682]	.001	.015
163	G_L	INS	4.246	0.529	[0.280, 0.776]	< .001	.002
164	G_R	INS	2.957	0.368	[0.122, 0.614]	.003	.049
172	dIg_R	INS	3.950	0.492	[0.244, 0.739]	< .001	.004
174	dId_R	INS	2.940	0.366	[0.120, 0.612]	.004	.049
182	A23v_R	CG	4.217	0.525	[0.276, 0.773]	< .001	.002
195	rLinG_L	MVOcC	3.985	0.496	[0.248, 0.743]	< .001	.004
197	vmPOS_L	MVOcC	4.668	0.581	[0.332, 0.830]	< .001	.001
198	vmPOS_R	MVOcC	3.263	0.406	[0.159, 0.652]	.001	.025
241	Otha_L	Tha	4.018	0.500	[0.252, 0.748]	< .001	.004
243	cTtha_L	Tha	2.938	0.366	[0.119, 0.612]	.004	.049

eTable 8. The network definition in Brainnetome atlas.

ID	Description	Subregion	Network	ID	Description	Subregion	Network
1	A8m	SFG_L_7_1	FPN	2	A8m	SFG_R_7_1	VAN
3	A8dl	SFG_L_7_2	DMN	4	A8dl	SFG_R_7_2	FPN
5	A9l	SFG_L_7_3	DMN	6	A9l	SFG_R_7_3	DMN
7	A6dl	SFG_L_7_4	DAN	8	A6dl	SFG_R_7_4	DAN
9	A6m	SFG_L_7_5	SMN	10	A6m	SFG_R_7_5	SMN
11	A9m	SFG_L_7_6	DMN	12	A9m	SFG_R_7_6	FPN
13	A10m	SFG_L_7_7	DMN	14	A10m	SFG_R_7_7	DMN
15	A9/46d	MFG_L_7_1	VAN	16	A9/46d	MFG_R_7_1	FPN
17	IFJ	MFG_L_7_2	FPN	18	IFJ	MFG_R_7_2	FPN
19	A46	MFG_L_7_3	FPN	20	A46	MFG_R_7_3	FPN
21	A9/46v	MFG_L_7_4	FPN	22	A9/46v	MFG_R_7_4	FPN
23	A8vl	MFG_L_7_5	DMN	24	A8vl	MFG_R_7_5	FPN
25	A6vl	MFG_L_7_6	DAN	26	A6vl	MFG_R_7_6	DAN
27	A10l	MFG_L_7_7	LIM	28	A10l	MFG_R_7_7	FPN
29	A44d	IFG_L_6_1	FPN	30	A44d	IFG_R_6_1	DAN
31	IFS	IFG_L_6_2	FPN	32	IFS	IFG_R_6_2	FPN
33	A45c	IFG_L_6_3	DMN	34	A45c	IFG_R_6_3	DMN
35	A45r	IFG_L_6_4	DMN	36	A45r	IFG_R_6_4	FPN
37	A44op	IFG_L_6_5	VAN	38	A44op	IFG_R_6_5	VAN
39	A44v	IFG_L_6_6	VAN	40	A44v	IFG_R_6_6	VAN
41	A14m	OrG_L_6_1	DMN	42	A14m	OrG_R_6_1	DMN
43	A12/47o	OrG_L_6_2	DMN	44	A12/47o	OrG_R_6_2	DMN
45	A11l	OrG_L_6_3	LIM	46	A11l	OrG_R_6_3	FPN
47	A11m	OrG_L_6_4	LIM	48	A11m	OrG_R_6_4	LIM
49	A13	OrG_L_6_5	LIM	50	A13	OrG_R_6_5	LIM
51	A12/47l	OrG_L_6_6	DMN	52	A12/47l	OrG_R_6_6	DMN
53	A4hf	PrG_L_6_1	SMN	54	A4hf	PrG_R_6_1	SMN
55	A6cdl	PrG_L_6_2	DAN	56	A6cdl	PrG_R_6_2	DAN
57	A4ul	PrG_L_6_3	SMN	58	A4ul	PrG_R_6_3	SMN
59	A4t	PrG_L_6_4	SMN	60	A4t	PrG_R_6_4	SMN
61	A4tl	PrG_L_6_5	VAN	62	A4tl	PrG_R_6_5	VAN
63	A6cvl	PrG_L_6_6	DAN	64	A6cvl	PrG_R_6_6	DAN
65	A1/2/3ll	PCL_L_2_1	VAN	66	A1/2/3ll	PCL_R_2_1	SMN
67	A4ll	PCL_L_2_2	SMN	68	A4ll	PCL_R_2_2	SMN
69	A38m	STG_L_6_1	LIM	70	A38m	STG_R_6_1	LIM
71	A41/42	STG_L_6_2	SMN	72	A41/42	STG_R_6_2	SMN
73	TE1.0/TE1.2	STG_L_6_3	SMN	74	TE1.0/TE1.2	STG_R_6_3	SMN
75	A22c	STG_L_6_4	SMN	76	A22c	STG_R_6_4	SMN
77	A38l	STG_L_6_5	LIM	78	A38l	STG_R_6_5	LIM

79	A22r	STG_L_6_6	DMN	80	A22r	STG_R_6_6	DMN
81	A21c	MTG_L_4_1	DMN	82	A21c	MTG_R_4_1	FPN
83	A21r	MTG_L_4_2	DMN	84	A21r	MTG_R_4_2	DMN
85	A37dl	MTG_L_4_3	DAN	86	A37dl	MTG_R_4_3	DAN
87	aSTS	MTG_L_4_4	DMN	88	aSTS	MTG_R_4_4	DMN
89	A20iv	ITG_L_7_1	LIM	90	A20iv	ITG_R_7_1	LIM
91	A37elv	ITG_L_7_2	DAN	92	A37elv	ITG_R_7_2	DAN
93	A20r	ITG_L_7_3	LIM	94	A20r	ITG_R_7_3	LIM
95	A20il	ITG_L_7_4	DMN	96	A20il	ITG_R_7_4	LIM
97	A37vl	ITG_L_7_5	DAN	98	A37vl	ITG_R_7_5	DAN
99	A20cl	ITG_L_7_6	FPN	100	A20cl	ITG_R_7_6	FPN
101	A20cv	ITG_L_7_7	LIM	102	A20cv	ITG_R_7_7	LIM
103	A20rv	FuG_L_3_1	LIM	104	A20rv	FuG_R_3_1	LIM
105	A37mv	FuG_L_3_2	VIS	106	A37mv	FuG_R_3_2	VIS
107	A37lv	FuG_L_3_3	DAN	108	A37lv	FuG_R_3_3	VIS
109	A35/36r	PhG_L_6_1	LIM	110	A35/36r	PhG_R_6_1	LIM
111	A35/36c	PhG_L_6_2	LIM	112	A35/36c	PhG_R_6_2	VIS
113	TL	PhG_L_6_3	VIS	114	TL	PhG_R_6_3	VIS
115	A28/34	PhG_L_6_4	LIM	116	A28/34	PhG_R_6_4	LIM
117	TI	PhG_L_6_5	LIM	118	TI	PhG_R_6_5	LIM
119	TH	PhG_L_6_6	VIS	120	TH	PhG_R_6_6	VIS
121	rpSTS	pSTS_L_2_1	DMN	122	rpSTS	pSTS_R_2_1	DMN
123	cpSTS	pSTS_L_2_2	VAN	124	cpSTS	pSTS_R_2_2	VAN
125	A7r	SPL_L_5_1	DAN	126	A7r	SPL_R_5_1	DAN
127	A7c	SPL_L_5_2	DAN	128	A7c	SPL_R_5_2	DAN
129	A5l	SPL_L_5_3	DAN	130	A5l	SPL_R_5_3	DAN
131	A7pc	SPL_L_5_4	SMN	132	A7pc	SPL_R_5_4	SMN
133	A7ip	SPL_L_5_5	DAN	134	A7ip	SPL_R_5_5	DAN
135	A39c	IPL_L_6_1	VIS	136	A39c	IPL_R_6_1	VIS
137	A39rd	IPL_L_6_2	FPN	138	A39rd	IPL_R_6_2	FPN
139	A40rd	IPL_L_6_3	DAN	140	A40rd	IPL_R_6_3	DAN
141	A40c	IPL_L_6_4	DMN	142	A40c	IPL_R_6_4	FPN
143	A39rv	IPL_L_6_5	DAN	144	A39rv	IPL_R_6_5	DMN
145	A40rv	IPL_L_6_6	SMN	146	A40rv	IPL_R_6_6	SMN
147	A7m	PCun_L_4_1	FPN	148	A7m	PCun_R_4_1	FPN
149	A5m	PCun_L_4_2	SMN	150	A5m	PCun_R_4_2	DAN
151	dmPOS	PCun_L_4_3	VIS	152	dmPOS	PCun_R_4_3	VIS
153	A31	PCun_L_4_4	DMN	154	A31	PCun_R_4_4	DMN
155	A1/2/3ulhf	PoG_L_4_1	SMN	156	A1/2/3ulhf	PoG_R_4_1	SMN
157	A1/2/3tonIa	PoG_L_4_2	SMN	158	A1/2/3tonIa	PoG_R_4_2	SMN
159	A2	PoG_L_4_3	DAN	160	A2	PoG_R_4_3	SMN

161	A1/2/3tru	PoG_L_4_4	SMN	162	A1/2/3tru	PoG_R_4_4	SMN
163	G	INS_L_6_1	SMN	164	G	INS_R_6_1	SMN
165	vIa	INS_L_6_2	SUB	166	vIa	INS_R_6_2	FPN
167	dIa	INS_L_6_3	VAN	168	dIa	INS_R_6_3	VAN
169	vId/vIg	INS_L_6_4	VAN	170	vId/vIg	INS_R_6_4	VAN
171	dIg	INS_L_6_5	SMN	172	dIg	INS_R_6_5	SMN
173	dId	INS_L_6_6	VAN	174	dId	INS_R_6_6	VAN
175	A23d	CG_L_7_1	DMN	176	A23d	CG_R_7_1	DMN
177	A24rv	CG_L_7_2	VAN	178	A24rv	CG_R_7_2	DMN
179	A32p	CG_L_7_3	DMN	180	A32p	CG_R_7_3	VAN
181	A23v	CG_L_7_4	DMN	182	A23v	CG_R_7_4	VIS
183	A24cd	CG_L_7_5	VAN	184	A24cd	CG_R_7_5	VAN
185	A23c	CG_L_7_6	VAN	186	A23c	CG_R_7_6	VAN
187	A32sg	CG_L_7_7	DMN	188	A32sg	CG_R_7_7	DMN
189	cLinG	MVOcC_L_5_1	VIS	190	cLinG	MVOcC_R_5_1	VIS
191	rCunG	MVOcC_L_5_2	VIS	192	rCunG	MVOcC_R_5_2	VIS
193	cCunG	MVOcC_L_5_3	VIS	194	cCunG	MVOcC_R_5_3	VIS
195	rLinG	MVOcC_L_5_4	VIS	196	rLinG	MVOcC_R_5_4	VIS
197	vmPOS	MVOcC_L_5_5	VIS	198	vmPOS	MVOcC_R_5_5	VIS
199	mOccG	LOcC_L_4_1	VIS	200	mOccG	LOcC_R_4_1	VIS
201	V5/MT+	LOcC_L_4_2	DAN	202	V5/MT+	LOcC_R_4_2	VIS
203	OPC	LOcC_L_4_3	VIS	204	OPC	LOcC_R_4_3	VIS
205	iOccG	LOcC_L_4_4	VIS	206	iOccG	LOcC_R_4_4	VIS
207	msOccG	LOcC_L_2_1	VIS	208	msOccG	LOcC_R_2_1	VIS
209	lsOccG	LOcC_L_2_2	VIS	210	lsOccG	LOcC_R_2_2	VIS
211	mAmyg	Amyg_L_2_1	SUB	212	mAmyg	Amyg_R_2_1	SUB
213	lAmyg	Amyg_L_2_2	SUB	214	lAmyg	Amyg_R_2_2	SUB
215	rHipp	Hipp_L_2_1	SUB	216	rHipp	Hipp_R_2_1	SUB
217	cHipp	Hipp_L_2_2	SUB	218	cHipp	Hipp_R_2_2	SUB
219	vCa	BG_L_6_1	SUB	220	vCa	BG_R_6_1	SUB
221	GP	BG_L_6_2	SUB	222	GP	BG_R_6_2	SUB
223	NAC	BG_L_6_3	SUB	224	NAC	BG_R_6_3	SUB
225	vmPu	BG_L_6_4	SUB	226	vmPu	BG_R_6_4	SUB
227	dCa	BG_L_6_5	SUB	228	dCa	BG_R_6_5	SUB
229	dlPu	BG_L_6_6	SUB	230	dlPu	BG_R_6_6	SUB
231	mPFtha	Tha_L_8_1	SUB	232	mPFtha	Tha_R_8_1	SUB
233	mPMtha	Tha_L_8_2	SUB	234	mPMtha	Tha_R_8_2	SUB
235	Stha	Tha_L_8_3	SUB	236	Stha	Tha_R_8_3	SUB
237	rTtha	Tha_L_8_4	SUB	238	rTtha	Tha_R_8_4	SUB
239	PPtha	Tha_L_8_5	SUB	240	PPtha	Tha_R_8_5	SUB
241	Otha	Tha_L_8_6	SUB	242	Otha	Tha_R_8_6	SUB

243	cTtha	Tha_L_8_7	SUB	244	cTtha	Tha_R_8_7	SUB
245	lPFtha	Tha_L_8_8	SUB	246	lPFtha	Tha_R_8_8	SUB

(Abbreviations: VIS, visual network; SMN, somatomotor network; DAN, dorsal attention network; VAN, ventral attention network; LIM, limbic network; FPN, frontoparietal network; DMN, default mode network; SUB, subcortical network)

eTable 9. Demographic characteristics of the matched sample. Wilcoxon rank sum test (Z) was used to analysis group differences of age and body mass index (BMI). χ^2 test was performed to analyze the gender differences. MAD: median absolute deviation.

Variables	**HCs (n = 101)**	**MDD (n = 168)**	**Statistical analysis**	***P* value**
Demographic variables				
Age (median [MAD], years)	14.8 [2.0]	15.9 [1.6]	$Z = 1.798$	.072
Gender (Male/Female)	40/61	32/69	$\chi_1^2 = 1.381$	.240
BMI (median [MAD], kg/m^2)	20.3 [2.4]	20.0 [2.3]	$Z = -0.738$	.461

eTable 10. Statistical analyses of SC−FC coupling differences among healthy controls, adolescent MDDs with and without suicidal attempt (SA+ and SA−). For abbreviations of anatomy and brain regions, please refer to eTable 1. Both FDR corrected p-value (P_{adj}) and original p-value (P) are provided.

ID	Subregion	Anatomy	*F*	Partial η^2	90% CI	*P*	P_{adj}
111	A35/36c_L	PhG	9.571	0.069	[0.025, 0.121]	< .001	.007
120	TH_R	PhG	7.620	0.056	[0.016, 0.104]	.001	.017
121	rpSTS_L	pSTS	6.421	0.048	[0.011, 0.093]	.002	.042
135	A39c_L	IPL	11.046	0.079	[0.031, 0.133]	< .001	.003
147	A7m_L	Pcun	6.201	0.046	[0.010, 0.091]	.002	.048
151	dmPOS_L	Pcun	6.547	0.048	[0.012, 0.094]	.002	.041
163	G_L	INS	9.007	0.066	[0.022, 0.116]	< .001	.007
172	dIg_R	INS	9.020	0.066	[0.022, 0.116]	< .001	.007
182	A23v_R	CG	9.050	0.066	[0.022, 0.117]	< .001	.007
195	rLinG_L	MVOcC	8.619	0.063	[0.002, 0.113]	< .001	.008
197	vmPOS_L	MVOcC	11.236	0.080	[0.032, 0.135]	< .001	.003
241	Otha_L	Tha	8.491	0.062	[0.020, 0.112]	< .001	.008

eTable 11. Post−hoc comparisons of SC−FC coupling differences among healthy controls, adolescent MDDs with and without suicidal attempt (SA+ and SA−). Both FDR corrected p-value (P_{adj}) and original p-value (P) are provided.

Subregion	Contrast	*T*	Cohen's *d*	95% CI	*P*	P_{adj}
A35/36c_L	SA− vs. HC	0.537	0.067	[−0.178, 0.312]	.853	.853
	SA+ vs. HC	−3.141	−0.392	[−0.638, −0.145]	.005	.008
	SA+ vs. SA−	−4.321	−0.539	[−0.787, −0.290]	< .001	< .001
TH_R	SA− vs. HC	3.868	0.483	[0.234, 0.730]	< .001	.001
	SA+ vs. HC	2.751	0.343	[0.097, 0.589]	.017	.026
	SA+ vs. SA−	−0.566	−0.071	[−0.315, 0.174]	.838	.838
rpSTS_L	SA− vs. HC	2.597	0.324	[0.078, 0.570]	.027	.040
	SA+ vs. HC	3.536	0.441	[0.193, 0.688]	.001	.004
	SA+ vs. SA−	1.654	0.206	[−0.039, 0.451]	.225	.225
A39c_L	SA− vs. HC	3.698	0.461	[0.213, 0.709]	.001	.001
	SA+ vs. HC	4.544	0.567	[0.317, 0.816]	< .001	< .001
	SA+ vs. SA−	1.764	0.220	[−0.025, 0.465]	.184	.184
A7m_L	SA− vs. HC	2.770	0.346	[0.099, 0.592]	.017	.025
	SA+ vs. HC	3.405	0.425	[0.177, 0.672]	.002	.007
	SA+ vs. SA−	1.323	0.165	[−0.08, 0.410]	.384	.384
dmPOS_L	SA− vs. HC	3.098	0.386	[0.139, 0.633]	.006	.009
	SA+ vs. HC	3.359	0.419	[0.172, 0.666]	.003	.008
	SA+ vs. SA−	0.939	0.117	[−0.128, 0.362]	.616	.616
G_L	SA− vs. HC	4.135	0.516	[0.267, 0.764]	< .001	< .001
	SA+ vs. HC	3.257	0.406	[0.159, 0.653]	.004	.005
	SA+ vs. SA−	−0.223	−0.028	[−0.272, 0.217]	.973	.973
dIg_R	SA− vs. HC	3.381	0.422	[0.174, 0.669]	.002	.004
	SA+ vs. HC	4.089	0.510	[0.261, 0.758]	< .001	.001
	SA+ vs. SA−	1.534	0.191	[−0.054, 0.436]	.277	.277
A23v_R	SA− vs. HC	3.882	0.484	[0.236, 0.732]	< .001	.001
	SA+ vs. HC	3.729	0.465	[0.217, 0.713]	.001	.001
	SA+ vs. SA−	0.598	0.075	[−0.170, 0.319]	.821	.821
rLinG_L	SA− vs. HC	3.512	0.438	[0.190, 0.685]	.002	.002
	SA+ vs. HC	3.884	0.485	[0.236, 0.732]	< .001	.001
	SA+ vs. SA−	1.156	0.144	[−0.101, 0.389]	.481	.481
vmPOS_L	SA− vs. HC	4.250	0.530	[0.281, 0.779]	< .001	< .001
	SA+ vs. HC	4.236	0.529	[0.279, 0.777]	< .001	< .001
	SA+ vs. SA−	0.840	0.105	[−0.140, 0.349]	.679	.679
Otha_L	SA− vs. HC	4.115	0.513	[0.264, 0.761]	< .001	< .001
	SA+ vs. HC	2.661	0.332	[0.085, 0.578]	.022	.034
	SA+ vs. SA−	−0.921	−0.115	[−0.360, 0.130]	.627	.627

eTable 12. Statistical analyses of SC−FC coupling differences among healthy controls, adolescent MDDs with and without non−suicidal self−injurious behaviors (NSSI+ and NSSI−). Both FDR corrected p-value (P_{adj}) and original p-value (P) are provided.

ID	Subregion	Anatomy	*F*	Partial η^2	90% CI	*P*	P_{adj}
22	A9/46v_R	MFG	8.225	0.061	[0.019, 0.110]	< .001	.010
86	A37dl_R	MTG	6.036	0.045	[0.010, 0.090]	.003	.048
120	TH_R	PhG	7.209	0.054	[0.015, 0.101]	.001	.020
135	A39c_L	IPL	10.367	0.075	[0.028, 0.129]	< .001	.005
151	dmPOS_L	Pcun	6.322	0.047	[0.011, 0.093]	.002	.040
163	G_L	INS	10.063	0.073	[0.027, 0.126]	< .001	.005
168	dIa_R	INS	8.189	0.060	[0.019, 0.110]	< .001	.010
172	dIg_R	INS	8.846	0.065	[0.022, 0.116]	< .001	.008
182	A23v_R	CG	8.915	0.065	[0.022, 0.116]	< .001	.008
195	rLinG_L	MVOcC	7.578	0.056	[0.016, 0.104]	.001	.016
197	vmPOS_L	MVOcC	11.805	0.085	[0.035, 0.140]	< .001	.003
198	vmPOS_R	MVOcC	7.002	0.052	[0.014, 0.099]	.001	.022
241	Otha_L	Tha	9.570	0.070	[0.025, 0.122]	< .001	.006
243	cTtha_L	Tha	8.283	0.061	[0.019, 0.111]	< .001	.010

eTable 13. Post−hoc comparisons of SC−FC coupling differences among healthy controls, adolescent MDDs with and without non−suicidal self−injurious behaviors (NSSI+ and NSSI−). Both FDR corrected p-value (P_{adj}) and original p-value (P) are provided.

Subregion	Contrast	*T*	Cohen's *d*	90% CI	*P*	P_{adj}
A9/46v_R	NSSI− vs. HC	4.029	0.505	[0.255, 0.753]	< .001	.001
	NSSI+ vs. HC	1.951	0.244	[−0.002, 0.491]	.127	.127
	NSSI+ vs. NSSI−	−2.477	−0.310	[−0.557, −0.063]	.037	.055
A37dl_R	NSSI− vs. HC	3.435	0.430	[0.182, 0.678]	.002	.006
	NSSI+ vs. HC	2.414	0.302	[0.055, 0.549]	.043	.065
	NSSI+ vs. NSSI−	−1.323	−0.166	[−0.411, 0.080]	.384	.384
TH_R	NSSI− vs. HC	3.215	0.403	[0.154, 0.650]	.004	.006
	NSSI+ vs. HC	3.509	0.440	[0.191, 0.688]	.002	.005
	NSSI+ vs. NSSI−	0.077	0.010	[−0.236, 0.255]	.997	.997
A39c_L	NSSI− vs. HC	4.306	0.539	[0.289, 0.789]	< .001	< .001
	NSSI+ vs. HC	3.701	0.464	[0.214, 0.712]	.001	.001
	NSSI+ vs. NSSI−	−0.948	−0.119	[−0.364, 0.127]	.611	.611
dmPOS_L	NSSI− vs. HC	3.178	0.398	[0.150, 0.646]	.005	.008
	NSSI+ vs. HC	3.141	0.393	[0.145, 0.641]	.005	.008
	NSSI+ vs. NSSI−	−0.270	−0.034	[−0.279, 0.212]	.961	.961
G_L	NSSI− vs. HC	4.309	0.540	[0.289, 0.789]	< .001	< .001
	NSSI+ vs. HC	3.514	0.440	[0.191, 0.688]	.002	.002
	NSSI+ vs. NSSI−	−1.149	−0.144	[−0.390, 0.102]	.485	.485
dIa_R	NSSI− vs. HC	3.779	0.473	[0.224, 0.722]	.001	.002
	NSSI+ vs. HC	1.010	0.127	[−0.119, 0.372]	.571	.571
	NSSI+ vs. NSSI−	−3.186	−0.399	[−0.647, −0.151]	.005	.007
dIg_R	NSSI− vs. HC	2.344	0.294	[0.046, 0.540]	.052	.078
	NSSI+ vs. HC	4.205	0.527	[0.276, 0.776]	< .001	< .001
	NSSI+ vs. NSSI−	1.787	0.224	[−0.023, 0.47]	.176	.176
A23v_R	NSSI− vs. HC	3.832	0.480	[0.231, 0.728]	< .001	.001
	NSSI+ vs. HC	3.666	0.459	[0.210, 0.707]	.001	.001
	NSSI+ vs. NSSI−	−0.453	−0.057	[−0.302, 0.189]	.893	.893
rLinG_L	NSSI− vs. HC	2.513	0.315	[0.067, 0.561]	.034	.050
	NSSI+ vs. HC	3.879	0.486	[0.236, 0.734]	< .001	.001
	NSSI+ vs. NSSI−	1.255	0.157	[−0.089, 0.403]	.422	.422
vmPOS_L	NSSI− vs. HC	3.526	0.442	[0.193, 0.690]	.001	.002
	NSSI+ vs. HC	4.768	0.597	[0.346, 0.847]	< .001	< .001
	NSSI+ vs. NSSI−	1.050	0.132	[−0.114, 0.377]	.546	.546
vmPOS_R	NSSI− vs. HC	2.181	0.273	[0.026, 0.520]	.076	.115
	NSSI+ vs. HC	3.742	0.469	[0.219, 0.717]	.001	.002
	NSSI+ vs. NSSI−	1.484	0.186	[−0.060, 0.432]	.300	.300

Otha_L	NSSI− vs. HC	4.359	0.546	[0.295, 0.795]	< .001	< .001
	NSSI+ vs. HC	2.833	0.355	[0.107, 0.602]	.014	.021
	NSSI+ vs. NSSI−	−1.921	−0.241	[−0.487, 0.006]	.135	.135
cTtha_L	NSSI− vs. HC	4.022	0.504	[0.255, 0.753]	< .001	.001
	NSSI+ vs. HC	1.820	0.228	[−0.018, 0.474]	.165	.165
	NSSI+ vs. NSSI−	−2.607	−0.326	[−0.573, −0.079]	.026	.039

eTable 14. Statistical analyses of SC−FC coupling differences among healthy controls, adolescent MDDs with and without childhood trauma (CT+ and CT−). Both FDR corrected p-value (P_{adj}) and original p-value (P) are provided.

ID	Subregion	Anatomy	*F*	Patial η^2	90% CI	*P*	P_{adj}
120	TH_R	PhG	7.723	0.059	[0.017, 0.109]	.001	.023
135	A39c_L	IPL	10.117	0.076	[0.028, 0.130]	< .001	.007
163	G_L	INS	8.360	0.063	[0.020, 0.115]	< .001	.017
172	dIg_R	INS	7.340	0.056	[0.016, 0.105]	.001	.028
182	A23v_R	CG	7.040	0.054	[0.014, 0.102]	.001	.033
195	rLinG_L	MVOcC	8.243	0.063	[0.019, 0.114]	< .001	.017
197	vmPOS_L	MVOcC	11.424	0.085	[0.034, 0.141]	< .001	.004
241	Otha_L	Tha	8.902	0.067	[0.022, 0.119]	< .001	.015

eTable 15. Post−hoc comparisons of SC−FC coupling differences among healthy controls, adolescent MDDs with and without childhood trauma (CT+ and CT−). Both FDR corrected p-value (P_{adj}) and original p-value (P) are provided.

Subregion	Contrast	*T*	Cohen's *d*	95% CI	*P*	P_{adj}
TH_R	CT− vs. HC	3.842	0.489	[0.235, 0.742]	< .001	.001
	CT+ vs. HC	3.015	0.384	[0.132, 0.635]	.008	.012
	CT+ vs. CT−	−1.212	−0.154	[−0.404, 0.096]	.447	.447
A39c_L	CT− vs. HC	4.140	0.527	[0.273, 0.780]	< .001	< .001
	CT+ vs. HC	3.933	0.500	[0.247, 0.753]	< .001	< .001
	CT+ vs. CT−	−0.555	−0.071	[−0.320, 0.179]	.844	.844
G_L	CT− vs. HC	3.223	0.410	[0.158, 0.662]	.004	.006
	CT+ vs. HC	3.966	0.505	[0.251, 0.758]	< .001	.001
	CT+ vs. CT−	0.559	0.071	[−0.178, 0.321]	.842	.842
dIg_R	CT− vs. HC	2.951	0.376	[0.124, 0.627]	.010	.015
	CT+ vs. HC	3.742	0.476	[0.223, 0.729]	.001	.002
	CT+ vs. CT−	0.633	0.081	[−0.169, 0.330]	.802	.802
A23v_R	CT− vs. HC	3.170	0.403	[0.151, 0.655]	.005	.007
	CT+ vs. HC	3.532	0.449	[0.196, 0.702]	.001	.004
	CT+ vs. CT−	0.146	0.019	[−0.231, 0.268]	.988	.988
rLinG_L	CT− vs. HC	3.830	0.487	[0.234, 0.740]	< .001	.001
	CT+ vs. HC	3.418	0.435	[0.182, 0.687]	.002	.003
	CT+ vs. CT−	−0.755	−0.096	[−0.346, 0.154]	.731	.731
vmPOS_L	CT− vs. HC	4.203	0.535	[0.281, 0.788]	< .001	< .001
	CT+ vs. HC	4.379	0.557	[0.302, 0.811]	< .001	< .001
	CT+ vs. CT−	−0.141	−0.018	[−0.267, 0.232]	.989	.989
Otha_L	CT− vs. HC	3.194	0.406	[0.154, 0.658]	.005	.007
	CT+ vs. HC	4.138	0.527	[0.272, 0.780]	< .001	< .001
	CT+ vs. CT−	0.782	0.100	[−0.150, 0.349]	.714	.714

eTable 16. Statistical analyses of SC−FC coupling differences among healthy controls, adolescent MDDs with and without major life events (MLE+ and MLE−). Both FDR corrected p-value (P_{adj}) and original p-value (P) are provided.

ID	Subregion	Anatomy	*F*	Patial η^2	90% CI	*P*	P_{adj}
13	A10m_L	SFG	8.92	0.068	[0.023, 0.121]	< .001	.007
23	A8vl_L	MFG	7.429	0.058	[0.016, 0.108]	.001	.017
41	A14m_L	OrG	6.977	0.054	[0.014, 0.103]	.001	.021
42	A14m_R	OrG	5.839	0.046	[0.010, 0.092]	.003	.036
86	A37dl_R	MTG	9.503	0.073	[0.026, 0.127]	< .001	.007
120	TH_R	PhG	6.573	0.051	[0.013, 0.099]	.002	.024
121	rpSTS_L	pSTS	5.795	0.046	[0.009, 0.091]	.003	.036
124	cpSTS_R	pSTS	6.047	0.047	[0.010, 0.094]	.003	.033
130	A5l_R	SPL	6.013	0.047	[0.010, 0.094]	.003	.033
135	A39c_L	IPL	9.500	0.073	[0.026, 0.127]	< .001	.007
147	A7m_L	Pcun	6.919	0.054	[0.014, 0.103]	.001	.021
151	dmPOS_L	Pcun	6.733	0.053	[0.013, 0.101]	.001	.022
153	A31_L	Pcun	6.751	0.053	[0.013, 0.101]	.001	.022
163	G_L	INS	7.309	0.057	[0.016, 0.106]	.001	.017
169	vId/vIg_L	INS	5.687	0.045	[0.009, 0.090]	.004	.038
172	dIg_R	INS	8.939	0.069	[0.023, 0.122]	< .001	.007
182	A23v_R	CG	8.625	0.066	[0.022, 0.119]	< .001	.008
187	A32sg_L	CG	8.427	0.065	[0.021, 0.117]	< .001	.009
195	rLinG_L	MVOcC	7.987	0.062	[0.019, 0.113]	< .001	.012
197	vmPOS_L	MVOcC	12.398	0.093	[0.039, 0.151]	< .001	.002
198	vmPOS_R	MVOcC	5.939	0.047	[0.010, 0.093]	.003	.034
214	lAmyg_R	Amyg	6.092	0.048	[0.011, 0.094]	.003	.033
234	mPMtha_R	Tha	7.757	0.060	[0.018, 0.111]	.001	.013
241	Otha_L	Tha	10.077	0.077	[0.028, 0.132]	< .001	.007
243	cTtha_L	Tha	6.086	0.048	[0.011, 0.094]	.003	.033

eTable 17. Post−hoc comparisons of SC−FC coupling differences among healthy controls, adolescent MDDs with and without major life events (MLE+ and MLE−). Both FDR corrected p-value (P_{adj}) and original p-value (P) are provided.

Subregion	Constrast	*T*	Cohen's *d*	95% CI	*P*	P_{adj}
A10m_L	MLE− vs. HC	−0.773	−0.099	[−0.351, 0.153]	.720	.720
	MLE+ vs. HC	2.743	0.352	[0.098, 0.605]	.018	.027
	MLE+ vs. MLE−	4.193	0.538	[0.281, 0.793]	< .001	< .001
A8vl_L	MLE− vs. HC	−1.268	−0.163	[−0.414, 0.089]	.415	.415
	MLE+ vs. HC	2.034	0.261	[0.008, 0.513]	.106	.160
	MLE+ vs. MLE−	3.853	0.494	[0.239, 0.749]	< .001	.001
A14m_L	MLE− vs. HC	−0.885	−0.114	[−0.365, 0.138]	.650	.650
	MLE+ vs. HC	2.266	0.291	[0.038, 0.543]	.063	.094
	MLE+ vs. MLE−	3.728	0.478	[0.223, 0.733]	.001	.002
A14m_R	MLE− vs. HC	−1.240	−0.159	[−0.411, 0.093]	.431	.431
	MLE+ vs. HC	1.697	0.218	[−0.035, 0.47]	.208	.313
	MLE+ vs. MLE−	3.410	0.437	[0.183, 0.691]	.002	.007
A37dl_R	MLE− vs. HC	2.239	0.287	[0.034, 0.540]	.067	.067
	MLE+ vs. HC	4.316	0.554	[0.297, 0.809]	< .001	< .001
	MLE+ vs. MLE−	2.897	0.372	[0.118, 0.625]	.011	.017
TH_R	MLE− vs. HC	3.430	0.440	[0.185, 0.694]	.002	.006
	MLE+ vs. HC	3.071	0.394	[0.140, 0.647]	.007	.010
	MLE+ vs. MLE−	0.092	0.012	[−0.240, 0.263]	.995	.995
rpSTS_L	MLE− vs. HC	2.742	0.352	[0.098, 0.605]	.018	.027
	MLE+ vs. HC	3.293	0.422	[0.168, 0.676]	.003	.010
	MLE+ vs. MLE−	1.102	0.141	[−0.111, 0.393]	.514	.514
cpSTS_R	MLE− vs. HC	2.024	0.260	[0.007, 0.512]	.109	.109
	MLE+ vs. HC	3.472	0.445	[0.19, 0.700]	.002	.005
	MLE+ vs. MLE−	2.090	0.268	[0.015, 0.520]	.094	.109
A5l_R	MLE− vs. HC	1.058	0.136	[−0.116, 0.387]	.541	.541
	MLE+ vs. HC	3.233	0.415	[0.160, 0.669]	.004	.012
	MLE+ vs. MLE−	2.833	0.363	[0.110, 0.617]	.014	.021
A39c_L	MLE− vs. HC	3.967	0.509	[0.253, 0.764]	< .001	.001
	MLE+ vs. HC	3.899	0.500	[0.244, 0.755]	< .001	.001
	MLE+ vs. MLE−	0.534	0.069	[−0.183, 0.320]	.855	.855
A7m_L	MLE− vs. HC	2.982	0.383	[0.128, 0.636]	.009	.013
	MLE+ vs. HC	3.604	0.462	[0.207, 0.717]	.001	.003
	MLE+ vs. MLE−	1.226	0.157	[−0.095, 0.409]	.439	.439
dmPOS_L	MLE− vs. HC	3.602	0.462	[0.207, 0.717]	.001	.003
	MLE+ vs. HC	2.809	0.360	[0.107, 0.614]	.015	.022
	MLE+ vs. MLE−	−0.413	−0.053	[−0.304, 0.199]	.910	.910

A31_L	MLE− vs. HC	0.640	0.082	[−0.170, 0.334]	.798	.798
	MLE+ vs. HC	3.216	0.413	[0.158, 0.666]	.004	.006
	MLE+ vs. MLE−	3.260	0.418	[0.164, 0.672]	.004	.006
G_L	MLE− vs. HC	3.294	0.423	[0.168, 0.676]	.003	.005
	MLE+ vs. HC	3.580	0.459	[0.204, 0.714]	.001	.004
	MLE+ vs. MLE−	0.863	0.111	[−0.141, 0.362]	.664	.664
vId/vIg_L	MLE− vs. HC	1.177	0.151	[−0.101, 0.403]	.468	.468
	MLE+ vs. HC	3.198	0.41	[0.156, 0.664]	.004	.013
	MLE+ vs. MLE−	2.662	0.341	[0.088, 0.594]	.023	.034
dIg_R	MLE− vs. HC	3.531	0.453	[0.198, 0.707]	.001	.002
	MLE+ vs. HC	4.029	0.517	[0.261, 0.772]	< .001	.001
	MLE+ vs. MLE−	1.159	0.149	[−0.103, 0.400]	.479	.479
A23v_R	MLE− vs. HC	3.615	0.464	[0.209, 0.718]	.001	.002
	MLE+ vs. HC	3.863	0.496	[0.240, 0.750]	< .001	.001
	MLE+ vs. MLE−	0.865	0.111	[−0.141, 0.363]	.663	.663
A32sg_L	MLE− vs. HC	−1.801	−0.231	[−0.483, 0.021]	.171	.194
	MLE+ vs. HC	1.737	0.223	[−0.030, 0.475]	.194	.194
	MLE+ vs. MLE−	4.060	0.521	[0.265, 0.776]	< .001	.001
rLinG_L	MLE− vs. HC	3.426	0.44	[0.185, 0.694]	.002	.003
	MLE+ vs. HC	3.754	0.482	[0.226, 0.736]	.001	.002
	MLE+ vs. MLE−	0.935	0.120	[−0.132, 0.372]	.619	.619
vmPOS_L	MLE− vs. HC	4.587	0.589	[0.331, 0.845]	< .001	< .001
	MLE+ vs. HC	4.390	0.563	[0.306, 0.819]	< .001	< .001
	MLE+ vs. MLE−	0.471	0.060	[−0.191, 0.312]	.885	.885
vmPOS_R	MLE− vs. HC	3.398	0.436	[0.181, 0.690]	.002	.007
	MLE+ vs. HC	2.583	0.331	[0.078, 0.584]	.028	.042
	MLE+ vs. MLE−	−0.472	−0.061	[−0.312, 0.191]	.884	.884
lAmyg_R	MLE− vs. HC	−1.169	−0.150	[−0.402, 0.102]	.473	.473
	MLE+ vs. HC	1.823	0.234	[−0.019, 0.486]	.164	.247
	MLE+ vs. MLE−	3.488	0.448	[0.192, 0.702]	.002	.005
mPMtha_R	MLE− vs. HC	1.181	0.152	[−0.100, 0.403]	.466	.466
	MLE+ vs. HC	3.664	0.470	[0.215, 0.725]	.001	.003
	MLE+ vs. MLE−	3.230	0.414	[0.160, 0.668]	.004	.006
Otha_L	MLE− vs. HC	2.977	0.382	[0.128, 0.635]	.009	.013
	MLE+ vs. HC	4.485	0.575	[0.318, 0.831]	< .001	< .001
	MLE+ vs. MLE−	2.312	0.297	[0.044, 0.549]	.056	.056
cTtha_L	MLE− vs. HC	2.421	0.311	[0.057, 0.563]	.043	.064
	MLE+ vs. HC	3.476	0.446	[0.191, 0.700]	.002	.005
	MLE+ vs. MLE−	1.669	0.214	[−0.038, 0.466]	.219	.219

eTable 18. Statistical analyses of SC−FC coupling differences among healthy controls, adolescent MDDs with and without major school bullying (SB+ and SB−). Both FDR corrected p-value (P_{adj}) and original p-value (P) are provided.

ID	Subregion	Anatomy	*F*	Patial η^2	90% CI	*P*	P_{adj}
120	TH_R	PhG	8.055	0.061	[0.019, 0.111]	< .001	.013
135	A39c_L	IPL	10.583	0.078	[0.030, 0.133]	< .001	.005
151	dmPOS_L	Pcun	7.320	0.056	[0.015, 0.104]	.001	.022
163	G_L	INS	9.332	0.070	[0.024, 0.122]	< .001	.007
172	dIg_R	INS	10.109	0.075	[0.028, 0.129]	< .001	.005
182	A23v_R	CG	8.703	0.065	[0.021, 0.117]	< .001	.008
195	rLinG_L	MVOcC	9.089	0.068	[0.023, 0.120]	< .001	.007
197	vmPOS_L	MVOcC	13.064	0.095	[0.042, 0.153]	< .001	.001
241	Otha_L	Tha	8.979	0.067	[0.023, 0.119]	< .001	.007

eTable 19. Post−hoc comparisons of SC−FC coupling differences among healthy controls, adolescent MDDs with and without major life events (SB+ and SB−). Both FDR corrected p-value (P_{adj}) and original p-value (P) are provided.

Subregion	Constrast	*T*	Cohen's *d*	95% CI	*P*	P_{adj}
TH_R	SB− vs. HC	3.720	0.471	[0.219, 0.723]	.001	.002
	SB+ vs. HC	3.509	0.445	[0.193, 0.696]	.002	.002
	SB+ vs. SB−	0.011	0.001	[−0.247, 0.250]	< .001	< .001
A39c_L	SB− vs. HC	4.322	0.548	[0.294, 0.800]	< .001	< .001
	SB+ vs. HC	3.941	0.500	[0.247, 0.751]	< .001	< .001
	SB+ vs. SB−	−0.149	−0.019	[−0.267, 0.230]	.988	.988
dmPOS_L	SB− vs. HC	3.359	0.426	[0.174, 0.677]	.003	.004
	SB+ vs. HC	3.535	0.448	[0.196, 0.699]	.001	.004
	SB+ vs. SB−	0.446	0.057	[−0.192, 0.305]	.896	.896
G_L	SB− vs. HC	3.942	0.500	[0.247, 0.751]	< .001	.001
	SB+ vs. HC	3.850	0.488	[0.235, 0.740]	< .001	.001
	SB+ vs. SB−	0.169	0.021	[−0.227, 0.270]	.984	.984
dIg_R	SB− vs. HC	4.496	0.570	[0.316, 0.823]	< .001	< .001
	SB+ vs. HC	2.830	0.359	[0.108, 0.609]	.014	.021
	SB+ vs. SB−	−1.669	−0.212	[−0.460, 0.038]	.219	.219
A23v_R	SB− vs. HC	3.702	0.469	[0.217, 0.721]	.001	.001
	SB+ vs. HC	3.822	0.484	[0.232, 0.736]	< .001	.001
	SB+ vs. SB−	0.404	0.051	[−0.197, 0.300]	.914	.914
rLinG_L	SB− vs. HC	4.243	0.538	[0.284, 0.790]	< .001	< .001
	SB+ vs. HC	2.990	0.379	[0.128, 0.629]	.009	.013
	SB+ vs. SB−	−1.195	−0.151	[−0.400, 0.098]	.458	.458
vmPOS_L	SB− vs. HC	4.246	0.538	[0.285, 0.791]	< .001	< .001
	SB+ vs. HC	4.881	0.619	[0.364, 0.872]	< .001	< .001
	SB+ vs. SB−	1.056	0.134	[−0.115, 0.382]	.542	.542
Otha_L	SB− vs. HC	4.217	0.535	[0.281, 0.787]	< .001	< .001
	SB+ vs. HC	2.970	0.376	[0.125, 0.627]	.009	.014
	SB+ vs. SB−	−1.189	−0.151	[−0.399, 0.098]	.461	.461

eTable 20. Partial Spearman correlation coefficients between SC−FC coupling and HAMD-17.

ID	Subregion	Anatomy	*r*	95% CI	*P*
6	A9l_R	SFG	−0.223	[−0.364, −0.072]	.004
14	A10m_R	SFG	−0.155	[−0.300, −0.003]	.050
18	IFJ_R	MFG	−0.211	[−0.352, −0.060]	.007
40	A44v_R	IFG	−0.186	[−0.330, −0.035]	.018
62	A4tl_R	PrG	0.156	[0.004, 0.301]	.048
86	A37dl_R	MTG	−0.163	[−0.308, −0.011]	.039
100	A20cl_R	ITG	−0.211	[−0.353, −0.060]	.007
130	A5l_R	SPL	−0.183	[−0.327, −0.032]	.020
132	A7pc_R	SPL	−0.171	[−0.315, −0.019]	.030
138	A39rd_R	IPL	−0.163	[−0.308, −0.011]	.039
188	A32sg_R	CG	−0.162	[−0.307, −0.010]	.040
191	rCunG_L	MVOcC	0.162	[0.010, 0.307]	.040
192	rCunG_R	MVOcC	0.208	[0.056, 0.350]	.008
194	cCunG_R	MVOcC	0.183	[0.031, 0.326]	.020
198	vmPOS_R	MVOcC	0.198	[0.046, 0.340]	.012
205	iOccG_L	LOcC	0.156	[0.004, 0.301]	.048
210	lsOccG_R	LOcC	0.183	[0.032, 0.327]	.020
212	mAmyg_R	Amyg	0.156	[0.004, 0.302]	.048

eTable 21. Partial Spearman correlation coefficients between SC−FC coupling and HAMA.

ID	Subregion	Anatomy	*r*	95% CI	*P*
6	A9l_R	SFG	−0.215	[−0.357, −0.064]	.006
14	A10m_R	SFG	−0.181	[−0.324, −0.029]	.022
16	A9/46d_R	MFG	−0.158	[−0.304, −0.006]	.045
18	IFJ_R	MFG	−0.247	[−0.386, −0.097]	.002
40	A44v_R	IFG	−0.271	[−0.408, −0.122]	< .001
42	A14m_R	OrG	−0.188	[−0.331, −0.036]	.017
62	A4tl_R	PrG	0.208	[0.056, 0.350]	.008
72	A41/42_R	STG	0.156	[0.004, 0.302]	.047
99	A20cl_L	ITG	−0.186	[−0.329, −0.034]	.018
120	TH_R	PhG	−0.181	[−0.325, −0.029]	.022
126	A7r_R	SPL	−0.170	[−0.314, −0.018]	.031
137	A39rd_L	IPL	−0.195	[−0.338, −0.043]	.013
138	A39rd_R	IPL	−0.173	[−0.317, −0.021]	.029
144	A39rv_R	IPL	−0.173	[−0.317, −0.021]	.028
153	A31_L	PCun	−0.173	[−0.317, −0.021]	.028
166	vIa_R	INS	−0.160	[−0.305, −0.008]	.042
167	dIa_L	INS	−0.157	[−0.302, −0.005]	.046
170	vId/vIg_R	INS	−0.188	[−0.331, −0.037]	.017
187	A32sg_L	CG	−0.177	[−0.321, −0.025]	.025
188	A32sg_R	CG	−0.203	[−0.345, −0.051]	.010

REFERENCES

1. Goñi J, van den Heuvel MP, Avena-Koenigsberger A, et al. Resting-brain functional connectivity predicted by analytic measures of network communication. *Proceedings of the National Academy of Sciences*. 2014/01/14 2014;111(2):833-838. doi:10.1073/pnas.1315529111
2. Bernstein DP, Ahluvalia T, Pogge D, Handelsman L. Validity of the Childhood Trauma Questionnaire in an adolescent psychiatric population. *J Am Acad Child Adolesc Psychiatry*. Mar 1997;36(3):340-8. doi:10.1097/00004583-199703000-00012
3. Huang D, Liu Z, Cao H, Yang J, Wu Z, Long Y. Childhood trauma is linked to decreased temporal stability of functional brain networks in young adults. *J Affect Disord*. Jul 1 2021;290:23-30. doi:10.1016/j.jad.2021.04.061
4. Van Dam NT, Rando K, Potenza MN, Tuit K, Sinha R. Childhood maltreatment, altered limbic neurobiology, and substance use relapse severity via trauma-specific reductions in limbic gray matter volume. *JAMA Psychiatry*. Aug 2014;71(8):917-25. doi:10.1001/jamapsychiatry.2014.680
5. Posner K, Brown GK, Stanley B, et al. The Columbia-Suicide Severity Rating Scale: initial validity and internal consistency findings from three multisite studies with adolescents and adults. *Am J Psychiatry*. Dec 2011;168(12):1266-77. doi:10.1176/appi.ajp.2011.10111704
6. Ulmer Yaniv A, Salomon R, Waidergoren S, Shimon-Raz O, Djalovski A, Feldman R. Synchronous caregiving from birth to adulthood tunes humans' social brain. *Proceedings of the National Academy of Sciences*. 2021/04/06 2021;118(14):e2012900118. doi:10.1073/pnas.2012900118
7. Esteban O, Markiewicz CJ, Blair RW, et al. fMRIPrep: a robust preprocessing pipeline for functional MRI. *Nat Methods*. 2019/01/01 2019;16(1):111-116. doi:10.1038/s41592-018-0235-4
8. Cieslak M, Cook PA, He X, et al. QSIPrep: an integrative platform for preprocessing and reconstructing diffusion MRI data. *Nat Methods*. 2021/07/01 2021;18(7):775-778. doi:10.1038/s41592-021-01185-5
9. Gorgolewski K, Burns C, Madison C, et al. Nipype: A Flexible, Lightweight and Extensible Neuroimaging Data Processing Framework in Python. Original Research. 2011-August-22 2011;5(13)doi:10.3389/fninf.2011.00013
10. Abraham A, Pedregosa F, Eickenberg M, et al. Machine learning for neuroimaging with scikit-learn. Methods. 2014-February-21 2014;8doi:10.3389/fninf.2014.00014
11. Garyfallidis E, Brett M, Amirbekian B, et al. Dipy, a library for the analysis of diffusion MRI data. *Front Neuroinform*. 2014;8:8. doi:10.3389/fninf.2014.00008
12. Tournier JD, Smith R, Raffelt D, et al. MRtrix3: A fast, flexible and open software framework for medical image processing and visualisation. *NeuroImage*. 2019/11/15/ 2019;202:116137. doi:https://doi.org/10.1016/j.neuroimage.2019.116137
13. Tustison NJ, Avants BB, Cook PA, et al. N4ITK: Improved N3 Bias Correction. *IEEE Transactions on Medical Imaging*. 2010;29(6):1310-1320. doi:10.1109/TMI.2010.2046908
14. Zhang Y, Brady M, Smith S. Segmentation of brain MR images through a hidden Markov random field model and the expectation-maximization algorithm. *IEEE Transactions on Medical Imaging*. 2001;20(1):45-57. doi:10.1109/42.906424
15. Fonov VS, Evans AC, McKinstry RC, Almli CR, Collins DL. Unbiased nonlinear average age-appropriate brain templates from birth to adulthood. *NeuroImage*. 2009/07/01/ 2009;47:S102. doi:https://doi.org/10.1016/S1053-8119(09)70884-5
16. Avants BB, Epstein CL, Grossman M, Gee JC. Symmetric diffeomorphic image registration with cross-correlation: Evaluating automated labeling of elderly and neurodegenerative brain. *Medical Image Analysis*. 2008/02/01/

2008;12(1):26-41. doi:https://doi.org/10.1016/j.media.2007.06.004
17. Jenkinson M, Bannister P, Brady M, Smith S. Improved Optimization for the Robust and Accurate Linear Registration and Motion Correction of Brain Images. *NeuroImage*. 2002/10/01/ 2002;17(2):825-841. doi:https://doi.org/10.1006/nimg.2002.1132
18. Cox RW, Hyde JS. Software tools for analysis and visualization of fMRI data. 1997;10(4-5):171-178. doi:https://doi.org/10.1002/(SICI)1099-1492(199706/08)10:4/5<171::AID-NBM453>3.0.CO;2-L
19. Wang S, Peterson DJ, Gatenby JC, Li W, Grabowski TJ, Madhyastha TM. Evaluation of Field Map and Nonlinear Registration Methods for Correction of Susceptibility Artifacts in Diffusion MRI. Original Research. 2017-February-21 2017;11doi:10.3389/fninf.2017.00017
20. Treiber JM, White NS, Steed TC, et al. Characterization and Correction of Geometric Distortions in 814 Diffusion Weighted Images. *PLOS ONE*. 2016;11(3):e0152472. doi:10.1371/journal.pone.0152472
21. Jenkinson M, Smith S. A global optimisation method for robust affine registration of brain images. *Medical Image Analysis*. 2001/06/01/ 2001;5(2):143-156. doi:https://doi.org/10.1016/S1361-8415(01)00036-6
22. Greve DN, Fischl B. Accurate and robust brain image alignment using boundary-based registration. *NeuroImage*. 2009/10/15/ 2009;48(1):63-72. doi:https://doi.org/10.1016/j.neuroimage.2009.06.060
23. Lanczos C. Evaluation of Noisy Data. *Journal of the Society for Industrial and Applied Mathematics Series B Numerical Analysis*. 1964/01/01 1964;1(1):76-85. doi:10.1137/0701007
24. Power JD, Mitra A, Laumann TO, Snyder AZ, Schlaggar BL, Petersen SE. Methods to detect, characterize, and remove motion artifact in resting state fMRI. *NeuroImage*. 2014/01/01/ 2014;84:320-341. doi:https://doi.org/10.1016/j.neuroimage.2013.08.048
25. Veraart J, Novikov DS, Christiaens D, Ades-Aron B, Sijbers J, Fieremans E. Denoising of diffusion MRI using random matrix theory. *Neuroimage*. Nov 15 2016;142:394-406. doi:10.1016/j.neuroimage.2016.08.016
26. Andersson JLR, Graham MS, Zsoldos E, Sotiropoulos SN. Incorporating outlier detection and replacement into a non-parametric framework for movement and distortion correction of diffusion MR images. *Neuroimage*. Nov 1 2016;141:556-572. doi:10.1016/j.neuroimage.2016.06.058
27. Behrens TE, Berg HJ, Jbabdi S, Rushworth MF, Woolrich MW. Probabilistic diffusion tractography with multiple fibre orientations: What can we gain? *Neuroimage*. Jan 1 2007;34(1):144-55. doi:10.1016/j.neuroimage.2006.09.018
28. Zamani Esfahlani F, Faskowitz J, Slack J, Mišić B, Betzel RF. Local structure-function relationships in human brain networks across the lifespan. *Nature Communications*. 2022/04/19 2022;13(1):2053. doi:10.1038/s41467-022-29770-y
29. Estrada E, Hatano N. Communicability in complex networks. *Physical review E, Statistical, nonlinear, and soft matter physics*. Mar 2008;77(3 Pt 2):036111. doi:10.1103/PhysRevE.77.036111
30. Hilgetag CC, Burns GA, O'Neill MA, Scannell JW, Young MP. Anatomical connectivity defines the organization of clusters of cortical areas in the macaque monkey and the cat. *Philosophical transactions of the Royal Society of London Series B, Biological sciences*. Jan 29 2000;355(1393):91-110. doi:10.1098/rstb.2000.0551
31. Seguin C, van den Heuvel MP, Zalesky A. Navigation of brain networks. 2018;115(24):6297-6302. doi:doi:10.1073/pnas.1801351115
32. Goñi J, Avena-Koenigsberger A, Velez de Mendizabal N, van den Heuvel MP, Betzel RF, Sporns O. Exploring the Morphospace of Communication Efficiency in Complex Networks. *PLOS ONE*. 2013;8(3):e58070. doi:10.1371/journal.pone.0058070
33. Betzel RF, Griffa A, Avena-Koenigsberger A, et al. Multi-scale community organization of the human structural connectome and its relationship with resting-state functional connectivity. *Network Science*. 2013;1(3):353-373. doi:10.1017/nws.2013.19

34. Lambiotte R, Sinatra R, Delvenne JC, Evans TS, Barahona M, Latora V. Flow graphs: Interweaving dynamics and structure. *Physical Review E*. 07/25/ 2011;84(1):017102. doi:10.1103/PhysRevE.84.017102
35. Ho D, Imai K, King G, Stuart EA. MatchIt: Nonparametric Preprocessing for Parametric Causal Inference. *Journal of Statistical Software*. 06/14 2011;42(8):1 - 28. doi:10.18637/jss.v042.i08
36. Váša F, Seidlitz J, Romero-Garcia R, et al. Adolescent Tuning of Association Cortex in Human Structural Brain Networks. *Cereb Cortex*. Jan 1 2018;28(1):281-294. doi:10.1093/cercor/bhx249
37. Alexander-Bloch AF, Shou H, Liu S, et al. On testing for spatial correspondence between maps of human brain structure and function. *Neuroimage*. Sep 2018;178:540-551. doi:10.1016/j.neuroimage.2018.05.070
38. Baller EB, Valcarcel AM, Adebimpe A, et al. Developmental coupling of cerebral blood flow and fMRI fluctuations in youth. *Cell Rep*. Mar 29 2022;38(13):110576. doi:10.1016/j.celrep.2022.110576